AD_ 296 194

63-2-4

Final Report F-B1857

DEVELOPMENT OF BROAD-BAND ELECTROMAGNETIC ABSORBERS FOR ELECTRO-EXPLOSIVE DEVICES

by

Paul F. Mohrbach
Robert F. Wood

June, 1961 to June, 1962

Prepared for

U.S. NAVAL WEAPONS LABORATORY
Dahlgren, Virginia
Code WHR

NWL NIPR 4-60
and
N178 - 7913

THE FRANKLIN INSTITUTE
LABORATORIES FOR RESEARCH AND DEVELOPMENT
PHILADELPHIA PENNSYLVANIA

THE FRANKLIN INSTITUTE • *Laboratories for Research and Development*

Final Report F-B1857

DEVELOPMENT OF BROAD-BAND ELECTROMAGNETIC ABSORBERS FOR ELECTRO-EXPLOSIVE DEVICES

by

Paul F. Mohrbach
Robert F. Wood

June, 1961 to June, 1962

Prepared for

U.S. NAVAL WEAPONS LABORATORY
Dahlgren, Virginia
Code WHR

NWL MIPR 4-60
and
N178 - 7913

ABSTRACT

This report contains a general description of the calculation of the complex ϵ^* and complex μ^* parameters of doughnut-shaped specimens from the measured quantities derived from our two measurement systems. The specific methods are referenced. The complex parameters as functions of frequency are presented in tabular form for a number of specimens. Characteristic plots of attenuation versus frequency are also included for 12 specimens. A brief discussion of our solution to a theoretical problem in the calculation (multivaluedness of the phase constant) is included.

A number of simple circuits were analyzed to determine how elemental components might introduce loss into a network. Resorting to use of an analog computer to aid in the manipulation of complex expressions led to a practical technique for designing a high loss network. Dissipative power loss in excess of 20 db at 20 kc and increasing on the order of 20 db or greater per decade is shown to be possible with components of practical value. However, for this loss to be realized in practice, the components would need to meet or exceed severe voltage or current specifications. Investigation of these requirements should be the prime consideration in the future pursuit of this study.

Studies of RF protective systems have led us to investigate some unusual materials and methods for eliminating unwanted RF energy. Electroluminescent phosphors, electroluminescent-photoconductive circuitry and dissipative filter networks were the topics studied. Phosphors do not at present form a probable solution to RF control, while electroluminescent-photoconductive circuitry and dissipative filters seem promising but require further development.

Our success with carbonyl iron resulted in a valuable contribution to the protection of ordnance devices from the hazards of electromagnetic radiation. However, it is limited in its effectiveness to frequencies of 100 Mc and up. Our experience has indicated that it is possible to obtain appreciable values of attenuation at frequencies of 1 Mc - 100 Mc by the use of a class of materials called ferrites. We have therefore conducted a study of ferrite materials as a major phase of the contract. Our study is divided into:

1. Material supply
2. Evaluation of samples for attenuating properties
3. Theoretical approach to attenuation
4. Methods of preparation of ferrites

We have been most fortunate in obtaining samples of ferrite toroids from commercial manufacturers. In order to reduce the number of samples to be evaluated to those which have values of electrical and magnetic parameters which are significant in maximizing losses, a literature study was made. A table showing electrical and magnetic properties of ferromagnetic materials which are available commercially is presented.

Samples of the ferrites, T-1, C-27, Q-1, and H-1 were received and evaluated. A composite plot of attenuation versus frequency is given which shows that C-27 is the best of the four for our purposes.

Inasmuch as our ultimate aim is to be able to specify the parameters that will maximize attenuation, an equation is given that relates attenuation to frequency, permittivity, permeability, and loss tangents. Two graphs are included which show the relationship of attenuation to frequency, with the products of real parts of complex relative permeability and complex relative permittivity as parameters with different values of loss tangents assumed.

Our literature study indicated that high initial permeability and low volume resistivity should be looked for. To aid in making a choice of a ferrite for further evaluation, two tables are given which list these properties for various powdered materials.

The method of preparation of ferrites is discussed. Some of the phenomena that might be exploited in making the material more lossy are mentioned.

Initial production of attenuators from fired ferrite powders are discussed and progress indicated.

In an effort to increase the resistance and voltage breakdown characteristics of RF-protected initiator assemblies, barium titanate ceramic tubes were evaluated as insulators. The ranges of insulation thickness and material dielectric constant required to provide insulated assemblies without appreciable loss in attenuation due to energy propagation through the dielectric were explored. For example, a ceramic insulator with a dielectric constant greater than 115 and a thickness of 0.017 inch produced no adverse effects on the assembly attenuation. A glass bonded mica with K = 7 and 0.010 thickness gave a 75% drop in attenuation compared to the uninsulated assembly. Some data irregularities in the attenuation change versus ceramic thickness and dielectric constant curves were noted. Measurements of the capacity and dissipation factor of the ceramic insulators, attenuating materials and assemblies were made to assist in the data evaluation.

A special sample group using small (1/16-inch outside diameter, 1/32-inch inside diameter) high K ceramic tubes was tested and no decreases in attenuation noted. Since application of ceramic preforms is impractical for many initiator designs, methods of applying thin coatings of high K insulation to initiator wires and the inner surfaces of initiator casings are recommended as a basis for further study.

Attempts to improve the attenuating ability of carbonyl iron attenuators were carried out during this contract. Two major phases were investigated: effect of particle size and effect of coating technique. Results of the particle size study were that 20 micron powder exhibited the best all around characteristics. Using 20 micron powder coated with 1/2% H_3PO_4, we were able to abtain samples that had 200 db/cm at 500 Mc.

Of the many coating techniques evaluated, only TiO_2 produced samples comparable to those made by the acetone-phosphate system. However, the TiO_2 system is much more complicated and does not have any special advantage.

There was one other phase of investigation; we tried using other powders (such as nickel and zinc) in place of the carbonyl iron. Success in this venture was nil.

TABLE OF CONTENTS

TABLE OF CONTENTS (Cont.)

LIST OF FIGURES

LIST OF FIGURES (Cont.)

LIST OF TABLES

1. INTRODUCTION

For several years, The Franklin Institute has been active in seeking solutions to problems concerning Hazards of Electromagnetic Radiation to Ordnance (HERO). Working under the sponsorship of the Naval Weapons Laboratory, we have striven to define the fundamental problems and then work towards their solutions. Research under these conditions has resulted in a more general understanding of the RF problem and has led to the development of an RF absorbing material (carbonyl iron) that can be made an integral part of an EED; that is, it can be used in place of the standard plug material. We also investigated the properties of a number of ferrite materials, for similar application.

The carbonyl iron material was developed under contract with Picatinny Arsenal and perfected under previous contracts with the Naval Weapons Laboratory and Picatinny Arsenal. Because it appeared that frequencies below 10 megacycles would give the most trouble, contrary to our first concern regarding radar frequency above 1000 megacycles, we have attempted to improve the iron's low frequency characteristics. As we gained more experience with attenuators made from carbonyl iron, it became apparent that by the use of this material we could not obtain enough attenuation below 100 Mc with the dimensional restrictions that were imposed. We therefore concentrated upon the family of materials called ferrites.

Results from the ferrite investigation are encouraging. From the data obtained during this project, it would seem that appreciable attenuation is attainable down to 1 Mc in a reasonable length of plug. Techniques by which the attenuation may be increased have been determined, and these suggest the direction for future work. There are, however, two disadvantages to ferrites which exhibit marked attenuation. First, they have low volume resistivity (ρ) which would shunt the dc input to the EED. For certain applications (such as low resistance devices) this may be unimportant. But to make the material of wider utility, we are investigating means of increasing resistivity.

The second disadvantage, far more serious than the first, is the fact that the ferrites cannot be molded in the same manner as the carbonyl iron. One of the main disadvantages of the carbonyl iron as an attenuating material is that it can be molded at room temperature into an EED plug with wire leads included. With ferrites, a curing temperature of 1400°C is required after molding. This eliminates the use of the two most commonly used lead wires: copper and stainless steel. Copper melts and stainless steel oxidizes severely.

Results obtained during this contract have pointed out the work required to make ferrite materials adaptable to EED's. The three major areas that still need further work are the following: dielectric coating on conductors to overcome low volume resistivity, method of molding ferrites at lower temperatures so that wire leads are not damaged, and preparation of ferrites "to order", to afford attenuation in any specified frequency range.

We have not limited our investigation to solid state attenuators but have also looked into the possibility of using filter networks having unconventional configurations. The possibility of using other less obvious energy-consuming phenomena such as electroluminescence, has also been examined.

During an investigation of this kind, the development of instrumentation for making the required measurements proceeds along with the project. This is especially true in work concerning RF where instrumentation is still in its infancy. In view of the amount of instrumentation that has been developed on this project and on previous contracts, we are not including it in this report. We shall prepare a separate report devoted entirely to instrumentation.

2. THEORETICAL AND PHYSICAL STUDIES

2.1 Determination of Sample Parameters

Contributor: Ramie H. Thompson

When the electrical behavior of a material (including attenuation) is specified in terms of its complex permittivity and permeability, the incremental transmission line model of the material preserves both a series and a shunt loss component. In general, the magnitude of the losses will be functions of the real part of the complex permittivity and permeability as well as the imaginary part of these parameters.

By evaluating many different materials in terms of μ^*, ϵ^*, and attenuation, an empirical method for maximizing attenuation by variation of component materials may be found. The data should also give insight into the division of the losses between series and shunt elements.

An alternative formulation for the description of electrical behavior may be made in terms of the three non-complex parameters ϵ, μ and σ. This formulation lumps all magnetic field losses with the electric field loss and does not preserve the series loss component in the incremental transmission line model. These parameters are related to the μ^*, ϵ^* parameters in a manner described in Appendix A.

The attenuation constant (α) as a function of the complex parameters is derived in Report P-B1857-6 on this project and is given by

$$\alpha = \frac{\omega}{\sqrt{2}} \sqrt{\mu_o \epsilon_o} \left[\epsilon''\mu'' - \epsilon'\mu' + \sqrt{\epsilon'^2\mu'^2 + \epsilon''^2\mu''^2 + \epsilon''^2\mu'^2 + \epsilon'^2\mu''^2} \right]^{1/2} \qquad (2\text{-}1)$$

where $\epsilon^* = \epsilon_o(\epsilon' - j\epsilon'')$ and $\mu^* = \mu_o(\mu' - j\mu'')$

Previous projects of The Franklin Institute Laboratories (A1992, A2301, A2358, A2479) had brought forth a measuring system for the determination of μ^* and ϵ^* for doughnut-shaped specimens. This

system, at the beginning of this project, was still handicapped by a multi-valuedness of one of the intermediate parameters (β) used in calculating μ^* and ϵ^*.

A detailed theoretical and physical description of the measurement system is contained in the Laboratories' Report P-A2301-14/P-A2358-8, (pp. 1-14). A discussion of the inherent errors of the system and a derivation of the equation necessary for programming the associated calculations for computer is presented in Report P-A2301-20/P-A2479-2. The accuracy of the system was checked by comparing measured parameters of Nylon, Teflon, and Polystyrene with published values. (See Report P-A2301-25/P-A2479-7).

Briefly, the system is used to find the input impedance to the sample under two values of terminating impedance; from this data, we can derive the characteristic impedance and propagation constant of the sample. The values of μ^* and ϵ^* are calculated from these last parameters. Determination of the input impedances of the specimen is indirect. The quantities that are actually measured are the location of the minimum points in the standing wave pattern on a uniform line in which the sample is mounted and also the ratio of maximum to minimum voltage of the standing wave pattern (VSWR). This measurement system we designate as the long line system.

The system was also limited in frequency range. Although measurements could be performed over the 500 Mc to 400 Mc range, reasonable accuracy could be obtained only in the vicinity of 500 Mc. The determination of the parameters at frequencies below 500 Mc was to be accomplished by a General Radio Immitance Bridge which directly measures input impedance, from 40 Mc to above 500 Mc. We planned to use the same system of calculation of μ^*, ϵ^* from the input impedances as described above for the long line system.

2.1.1 Unique Determination of the Phase Constant

As previously mentioned, the calculation of μ^* and ϵ^* from the data (from either measurement system) was not unique because the phase

constant, β, was multivalued. A complete description of how this multivaluedness arises and the approaches used to solve the problem are given in our Reports P-A2301-26/P-A2479-8 and P-A2301-37/P-A2479-9/P-B1857-1.

According to the method we adopted, we solve the problem by measuring the normally required data for the μ^*, ϵ^*, computation at two frequencies within a few percent of each other. If we make the assumption that the μ^*, ϵ^* parameters are slowly varying functions of frequency over this interval, we can then determine the actual value of β by computation. The assumption of slowly varying μ^*, ϵ^* parameters is justified by our previous determinations of the attenuation constant of carbonyl iron doughnuts. These measurements were performed on our matched attenuation determination system (not the system we are discussing here). Examples can be found in Report P-A2479-13/P-B1857-5 where it is shown that most of the carbonyl iron samples have a curve of attenuation versus frequency having the form $\alpha = K\omega^{4/3}$. (2-2)

Now α can be expressed as

$$\alpha = \mathrm{Re}\ \{ -j\omega\ \mu^*\epsilon^* \} \qquad (2\text{-}3)$$

Comparison of this equation with equation (2-2) shows that $\mathrm{Re}\ \{ -j\ \mu^*\epsilon^* \}$ is directly proportional to $\omega^{1/3}$, which varies less than 2% over a frequency variation of 5%. With the phase constant uniquely determined, we were ready for actual measurements. Twenty samples of varying attenuation were measured at 500 and 525 Mc. The results are given in Table 2-1.

Table 2-1

PARAMETERS FOR SAMPLES R-101 THRU R-120, AT 500 MC

	$\alpha N/M$	$Re\mu$	$Im\mu$	$Re\epsilon$	$Im\epsilon$
R101	128	8.0	-5.9	109	-13
R103	96.4	7.2	-7.4	83	14
R104	122	8.1	-5.3	123	-13
R106	323	12.7	-8.4	321	-102
R107	268	11.4	-7.6	288	-69
R108	221	7.8	6.4	277	-35
R109	304	11.7	-7.7	301	-100
R110	284	10.9	-7.3	341	-79
R111	601	16.7	-12	708	-246
R112	510	14.7	-10.9	697	-17
R113	517	7.3	-8.2	641	-244
R114	476	14.4	-10	746	-145
R115	454	14.7	-9.5	729	-150
R117	576	16.6	-12.3	1011	-141
R118	731	15.6	-14.4	1014	-240
R119	599	14.3	-11.3	1113	-211
R120	528	17.3	-11.4	1013	-126

2.1.2 The Immittance Bridge System

The General Radio Immittance Bridge 1607A was used to determine sample parameters from 40 Mc to 400 Mc. The sample holder used with this system was the same one used with the long line system. The largest single source of error in either system was the sample holder. This holder had been modified at least six times before absolutely repeatable data could be obtained. Wishing to avoid this kind of trouble with the immittance bridge system, we continued the use of the long line sample holder.

The computer program used to compute μ^* and ϵ^* from the long line data was modified to accept the input impedance data obtained from the immittance bridge.

Since the long line system had been checked for accuracy against published data, we compared immittance bridge determinations

of parameters at 500 Mc with those determined by the long line system at that frequency.

Table 2-2 shows the results.

We felt that the agreement was close enough to use the immittance bridge to determine roughly the sample parameters over the range of 40 to 500 Mc. At this time we also were using the immittance bridge system as our only method of determining attenuation below 150 Mc. Table 2-2 shows that although parameter measurements are not identical on the two systems, the attenuations measured in db are within a few percent of each other. We therefore felt that the immittance bridge would give accurate attenuation readings over the 40 Mc to 500 Mc band. Tables 2-3 to 2-14 show the parameters of 12 samples as a function of frequency. Figures 2-1, and 2-2, and 2-3 show the attenuation of the same samples as a function of frequency. In these figures the X's represent data points obtained from the long line system or the immittance bridge. The circles are the attenuations as determined by our matched attenuation determining system. This system lumps losses in the matching systems with losses in the sample and therefore always reads high. Note also that both immittance bridge and long line system measurements were made at 500 and 525 Mc. The close grouping of the X's at these frequencies is a measure of system agreement.

A combination of Figures 2-1 to 2-3 gives Figure 2-4 which shows the uniformity of the individual, groups of samples. Sample groups (Figure 2-4) 1 and 2 were made from different carbonyl iron powders.

Table 2-2

PARAMETERS MEASUREMENTS

Sample No.	freq. (mc)	N	Parameters Measured on Long Line: α nepers meter	α db cm	Re. μ*	Im. μ*	Re. ε*	Im. ε*	Parameters Measured on Immittance Bridge: α nepers meter	α db cm	Re. μ*	Im. μ*	Re. ε*	Im. ε*
R-114	500	0	473	41.2	12.5	-10.4	786	-97.0	423	36.8	12.0	-8.75	822	-96.0
	525	0	483	41.9	12.7	-8.70	809	-161	453	39.3	11.7	-9.07	787	-96.0
R-119	500	1	605	52.6	14.5	-11.2	1218	-164	668	58.0	14.2	-12.1	1280	-180
	525	1	636	55.2	14.0	-10.4	1235	-206	606	52.6	13.7	-10.4	1260	-146
R-139	500	0	346	30.8	11.5	-9.00	505	-61.0	337	29.3	10.8	-9.30	513	-31.0
	525	0	344	29.9	11.3	-8.50	508	-53.0	333	28.9	11.1	-8.40	512	-41.0
R-117	500	1	618	53.7	14.6	-11.2	1171	-186	602	52.3	13.9	-11.0	1240	-147
	525	1	682	59.3	14.1	-10.7	1174	-271	604	52.4	14.1	-10.5	1200	-154
R-120	500	1	606	52.6	14.8	-10.9	1232	-187	568	49.3	13.4	-10.7	1300	-84.0
	525	1	630	54.7	14.4	-10.1	1279	-210	624	54.2	13.9	-10.6	1280	-154
R-140	500	0	334	29.0	18.0	-10.0	423	+.160	307	26.7	7.50	-9.80	410	+30.0
	525	0	356	31.0	7.7	-9.40	437	-15.1	350	30.4	8.00	-9.50	425	-15.9
R-142	500	0	529	46.0	14.0	-11.1	723	-174	540	46.9	12.3	-12.4	717	-119
	525	0	564	49.0	13.3	-11.1	723	-177	564	48.0	13.2	-11.2	697	-176
R-143	500	0	482	41.8	14.0	-10.4	764	-137	484	42.1	13.0	-11.6	772	-66.0
	525	0	619	53.8	13.0	-13.9	848	-84.0	582	50.7	-3.80	-7.80	223	-24.0

Table 2-3

"PARAMETERS FOR SAMPLE #5819"

Freq. in Mc	Re μ*	Im μ*	Re ε*	Im ε*	ReZ_0	ImZ_0
525	13.0	- 9.11	864	- 149	6.57	- 1.46
500*	13.8	- 9.67	833	- 154	6.89	- 1.49
525	12.0	- 8.99	890	- 112	6.25	- 1.65
500	12.2	- 8 93	9o2	- 110	6.21	- 1.61
236	17.4	- 9.95	931	- 86.1	7.16	- 1.54
225	17.9	- 10.1	931	- 94.7	7.25	- 1.53
99	24.2	- 7.99	1018	- 116	7.85	- 0.803
95	24.3	- 7.45	1031	- 112	7.79	- 0.739
42	26.5	- 3.50	1039	- 135	7.99	- 0.008
40	27.0	- 4.95	1099	- 167	7.85	- 0.119

Table 2-4

"PARAMETERS FOR SAMPLE #5820"

Freq. in Mc	Re μ*	Im μ*	Re ε*	Im ε*	ReZ_0	ImZ_0
525*	11.8	- 9.26	883	- 117	6.27	- 1.70
500*	12.8	- 9.72	848	- 120	6.64	- 1.72
525	10.0	- 8.90	946	- 137	5.85	- 1.61
500	11.0	- 8.85	969	- 114	5.79	- 1.65
236	16.9	- 10.9	939	- 43.1	7.06	- 1.91
225	17.1	- 10.9	955	- 42.7	7.03	- 1.88
99	24.2	- 8.23	1022	- 99.1	7.83	- 0.909
95	24.2	- 7.47	1018	- 85.6	7.86	- 0.839
42	28.5	- 3.81	1077	- 155	8.13	+ 0.044
40	26.7	- 2.42	1095	- 158	7.78	+ 0.209

*Parameters Determined By Long Line System

Table 2-5

"PARAMETERS FOR SAMPLE #5821"

Freq. in Mc	Re μ^*	Im μ^*	Re ϵ^*	Im ϵ^*	ReZ_0	ImZ_0
525*	12.9	- 8.64	873	- 142	6.48	- 1.40
500*	13.9	- 9.26	856	- 149	6.78	- 1.43
525	12.6	- 8.52	924	- 133	6.22	- 1.42
500	12.3	- 8.56	937	- 107	6.12	- 1.53
236	17.9	- 10.0	947	- 92.1	7.19	- 1.51
225	18.2	- 10.7	950	- 71.9	7.25	- 1.69
99	24.5	- 8.05	1043	- 114	7.80	- 0.812
95	24.6	- 7.37	1056	- 97.8	7.74	- 0.771
42	28.8	- 4.33	1115	- 158	8.04	- 0.0320
40	16.7	- 2.30	607	- 82.9	8.30	- 0.00370

Table 2-6

"PARAMETERS FOR SAMPLE #5822"

Freq. in Mc	Re μ^*	Im μ^*	Re ϵ^*	Im ϵ^*	ReZ_0	ImZ_0
525*	11.6	- 9.08	869	- 113	6.25	- 1.70
500*	12.9	- 10.5	859	- 96.5	6.65	- 1.96
525	11.0	- 8.91	898	- 89.2	6.01	- 1.79
500	11.1	- 8.93	906	- 93.3	6.00	- 1.76
236	16.5	- 10.7	929	- 42.8	7.02	- 1.90
225	16.7	- 11.3	917	- 37.1	7.14	- 1.20
99	23.5	- 7.21	1003	- 62.7	7.77	- 0.916
95	23.2	- 4.18	1420	- 532	6.20	+ 0.560
42	26.3	- 3.55	1077	- 123	7.82	- 0.9774
40	27.6	- 3.28	1063	- 155	8.05	+ 0.109

*Parameters Determined By Long Line System

Table 2-7

"PARAMETERS FOR SAMPLE #5824"

Freq. in Mc	Re μ*	Im μ*	Re ε*	Im ε*	ReZ_0	ImZ_0
525*	14.3	- 10.2	1290	- 202	5.64	- 1.33
500*	14.7	- 11.3	1244	- 172	5.87	- 1.56
525	12.8	- 9.39	1393	- 197	5.16	- 1.28
500	13.0	- 9.91	1408	- 110	5.17	- 1.51
236	19.0	- 12.7	1368	- 99.9	6.24	- 1.64
225	19.5	- 12.4	1373	- 99.5	6.29	- 1.54
99	29.0	- 11.0	1472	- 136	7.18	- 0.979
95	29.5	- 10.2	1476	- 158	7.20	- 0.828
42	34.4	- 5.02	1521	- 210	7.52	- 0.0270
40	35.7	- 4.46	1566	- 230	7.53	- 0.0816

Table 2-8

"PARAMETERS FOR SAMPLE #5825"

Freq. in Mc	Re μ*	Im μ*	Re ε*	Im ε*	ReZ_0	ImZ_0
525*	15.2	- 10.6	1237	- 223	5.93	- 1.29
500*	15.6	- 11.95	1223	- 168	6.10	- 1.60
525	13.8	- 9.56	1364	- 231	5.38	- 1.19
500	13.9	- 10.3	1372	- 113	5.39	- 1.54
236	20.3	- 12.5	1332	- 147	6.51	- 1.46
225	20.7	- 12.4	1339	- 145	6.54	- 1.43
99	29.5	- 9.95	1485	- 205	7.18	- 0.673
95	29.8	- 9.78	1486	- 197	7.20	- 0.667
42	36.8	- 4.88	1438	- 272	7.96	+ 0.221
40	35.5	- 5.33	1601	- 234	7.45	- 0.0126

*Parameters Determined By Long Line System

Table 2-9

"PARAMETERS FOR SAMPLE #5826"

Freq. in Mc	Re μ*	Im μ*	Re ε*	Im ε*	ReZ$_0$	ImZ$_0$
525*	14.4	- 11.0	1245	- 223	5.82	- 1.40
500*	15.5	- 11.6	1211	- 164	6.09	- 1.58
525	13.6	- 9.48	1360	- 232	5.36	- 1.19
500	13.6	- 10.3	1373	- 141	5.36	- 1.51
236	20.3	- 12.5	1327	- 150	6.53	- 1.45
225	20.7	- 12.3	1341	- 150	6.53	- 1.45
99	28.1	- 10.7	1540	- 65.6	6.89	- 1.11
95	28.9	- 10.1	1558	- 102	6.94	- 0.950
42	36.6	- 4.94	1528	- 220	7.73	+ 0.0361
40	35.1	- 3.70	1594	- 239	7.39	- 0.163

Table 2-10

"PARAMETERS FOR SAMPLE #5827"

Freq. in Mc	Re μ*	Im μ*	Re ε*	Im ε*	ReZ$_0$	ImZ$_0$
525*	13.1	- 12.0	1263	- 488	5.64	- 1.14
500*	14.8	- 11.4	1241	- 190	5.92	- 1.52
525	13.3	- 9.65	1386	- 204	5.26	- 1.29
500	13.4	- 10.3	1400	- 121	5.26	- 1.54
236	19.6	- 12.5	1352	- 115	6.36	- 1.56
225	19.5	- 12.2	1377	- 120	6.28	- 1.50
99	28.9	- 10.6	1424	- 133	7.15	- 0.948
95	79.4	- 10.3	1490	- 137	7.17	- 0.885
42	35.2	- 5.89	1527	- 192	7.62	- 0.153
40	35.3	- 4.18	1570	- 219	7.48	- 0.0788

*Parameters Determined By Long Line System

Table 2-11

"PARAMETERS FOR SAMPLE #5799"

Freq. in Mc	Re μ*	Im μ*	Re ε*	Im ε*	ReZ_0	ImZ_0
236	16.0	- 17.4	3967	- 470	3.61	- 1.34
225	15.8	- 18.3	4027	- 565	3.61	- 1.36
157	21.6	- 20.2	4182	- 427	4.27	- 1.33
150	21.90	- 20.1	4154	- 506	4.01	- 1.29
73	36.0	- 20.2	4222	- 276	4.81	- 1.09
70	36.7	- 21.6	4202	- 129	3.97	- 1.27
42	130.0	- 0.22	11080	- 1801	5.37	+ 0.429
40	136.0	+ 34.2	12050	- 1811	5.26	+ 0.460

Table 2-12

"PARAMETERS FOR SAMPLE #5800"

Freq. in Mc	Re μ*	Im μ*	Re ε*	Im ε*	ReZ_0	ImZ_0
236	16.6	- 17.8	4472	- 551	3.45	- 1.25
225	15.8	- 19.3	4471	- 549	3.45	- 1.38
157	21.7	- 20.8	4446	- 448	3.88	- 1.33
150	22.1	- 20.2	4457	- 350	3.87	- 1.37
73	36.0	- 21.0	4365	- 237	4.75	- 1.14
70	37.2	- 21.5	4396	- 151	4.79	- 1.20
42	128	+ 1.47	11065	- 1930	5.32	+ 0.491
40	138	+ 1.80	11691	- 1865	5.38	+ 0.461

*Parameters Determined By Long Line System

Table 2-13

"PARAMETERS FOR SAMPLE #5801"

Freq. in Mc	Re μ*	Im μ*	Re ε*	Im ε*	ReZ_0	ImZ_0
236	20.5	- 19.0	4005	- 422	3.95	- 1.31
225	20.4	- 20.2	3960	- 407	4.00	- 1.41
157	26.5	- 21.7	4177	- 500	4.33	- 1.26
150	27.3	- 20.9	4026	- 558	4.45	- 1.17
73	38.6	- 14.2	4588	- 881	4.67	- 0.383
70	40.3	- 15.2	4570	- 872	4.79	- 0.416
42	119	- 1.20	11873	- 1860	4.96	+ 0.361
40	127	+ 0.662	12713	- 1840	4.97	+ 0.371

Table 2-14

"PARAMETERS FOR SAMPLE #5802"

Freq. in Mc	Re μ*	Im μ*	Re ε*	Im ε*	ReZ_0	ImZ_0
236	16.0	- 18.9	3959	- 599	3.68	- 1.38
225	17.8	- 20.3	4058	- 576	3.81	- 1.41
157	23.5	- 21.7	4274	- 663	4.11	- 1.25
150	22.8	- 19.9	4195	- 742	4.06	- 1.12
73	35.8	- 20.0	4403	- 356	4.70	- 1.02
70	38.6	- 20.3	4261	- 435	4.96	- 0.962
42	130	- 0.335	11272	- 1794	5.32	+ 0.414
40	137	- 1.97	12106	- 1982	5.26	+ 0.466

*Parameters Determined By Long Line System

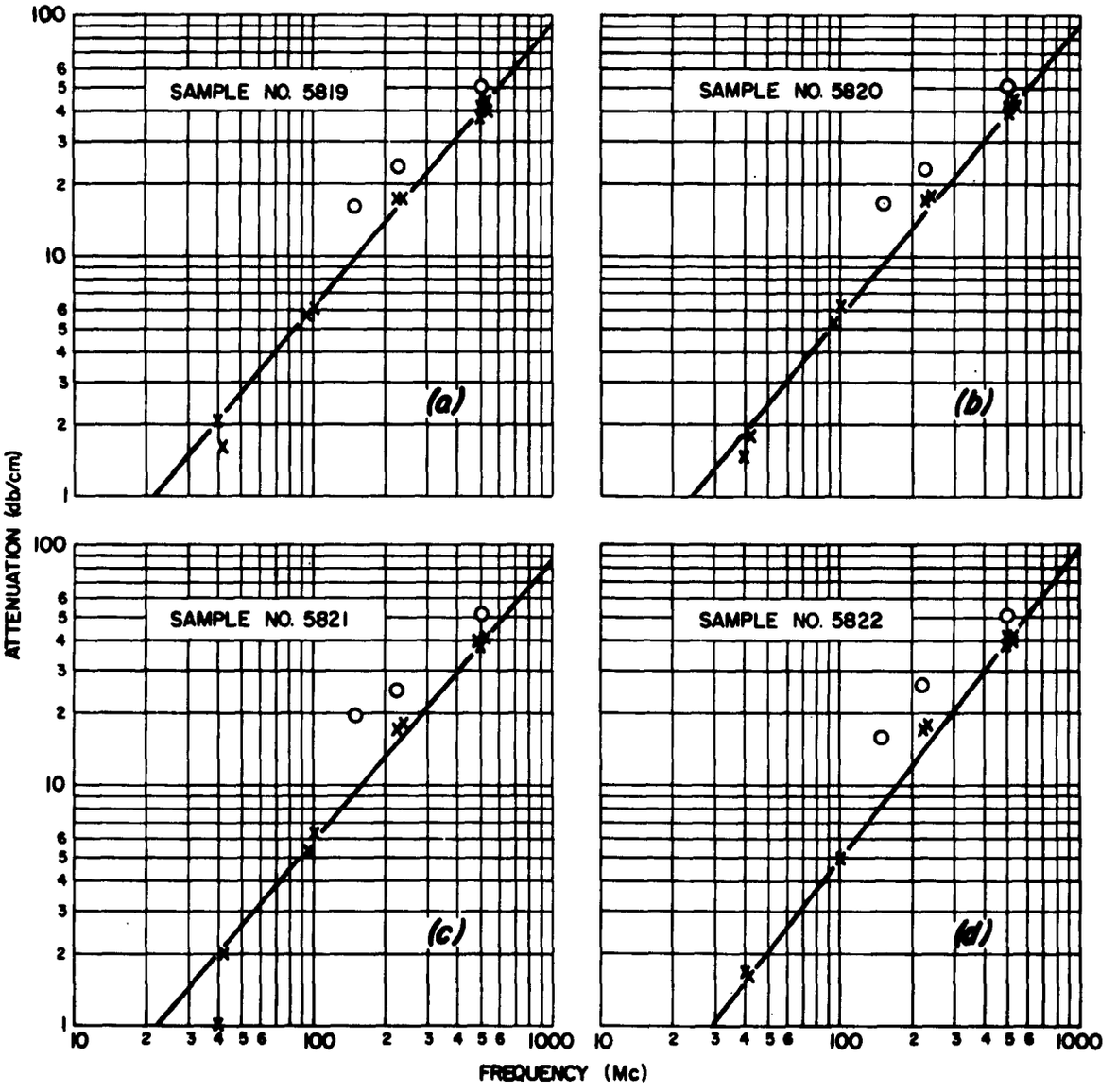

FIG. 2-1. ATTENUATION VERSUS FREQUENCY

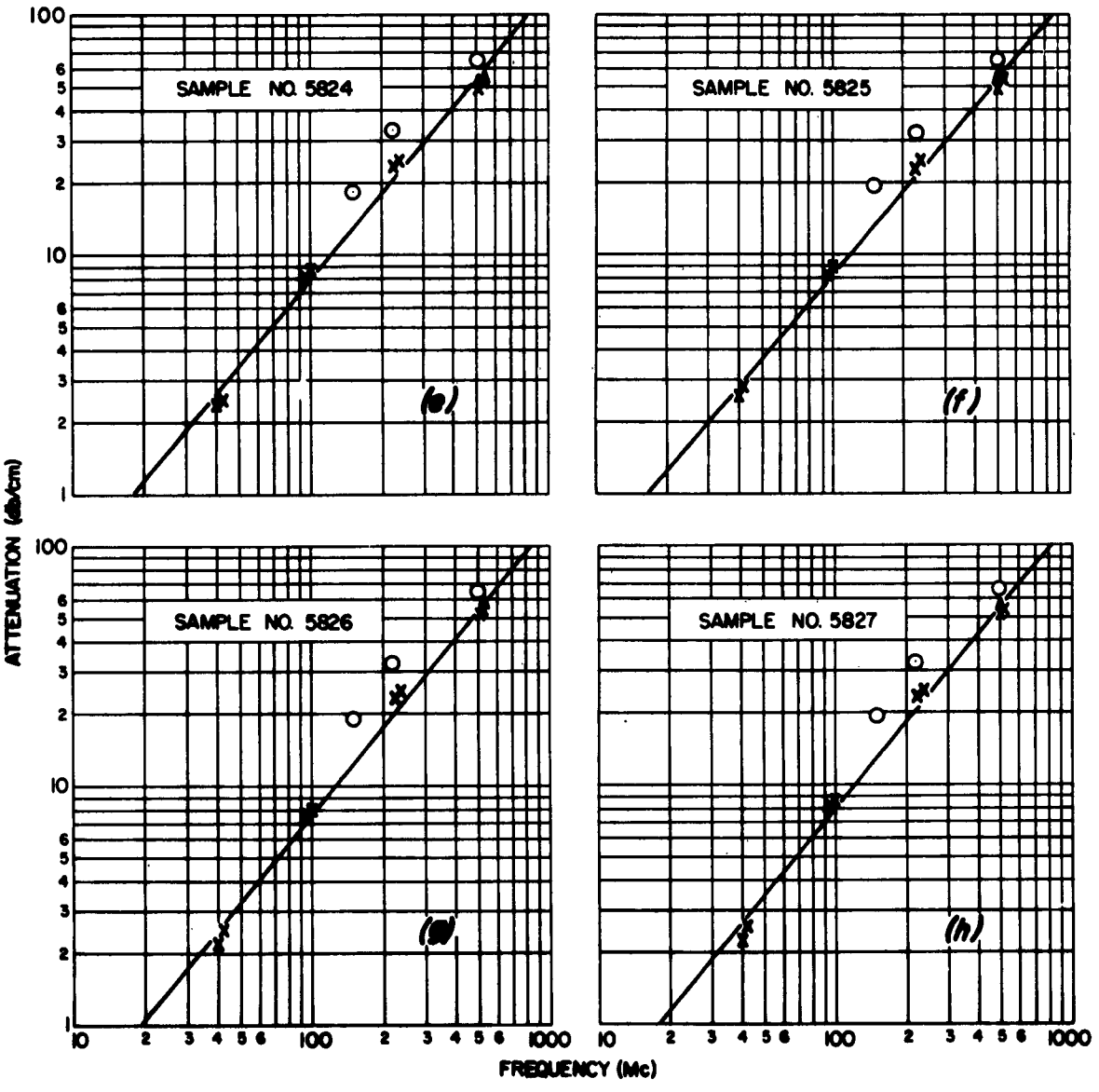

FIG. 2-2. ATTENUATION VERSUS FREQUENCY

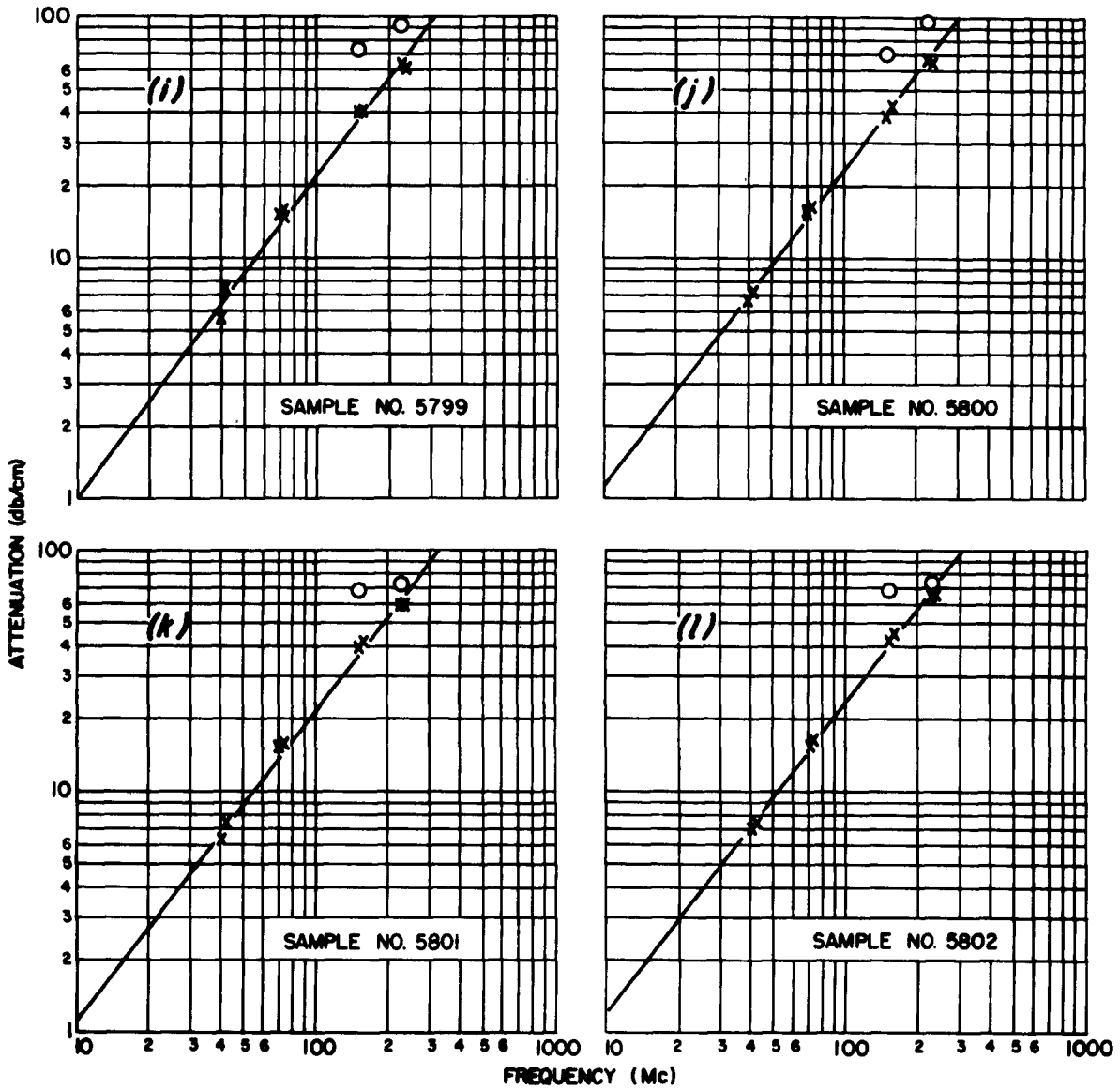

FIG. 2-3. ATTENUATION VERSUS FREQUENCY

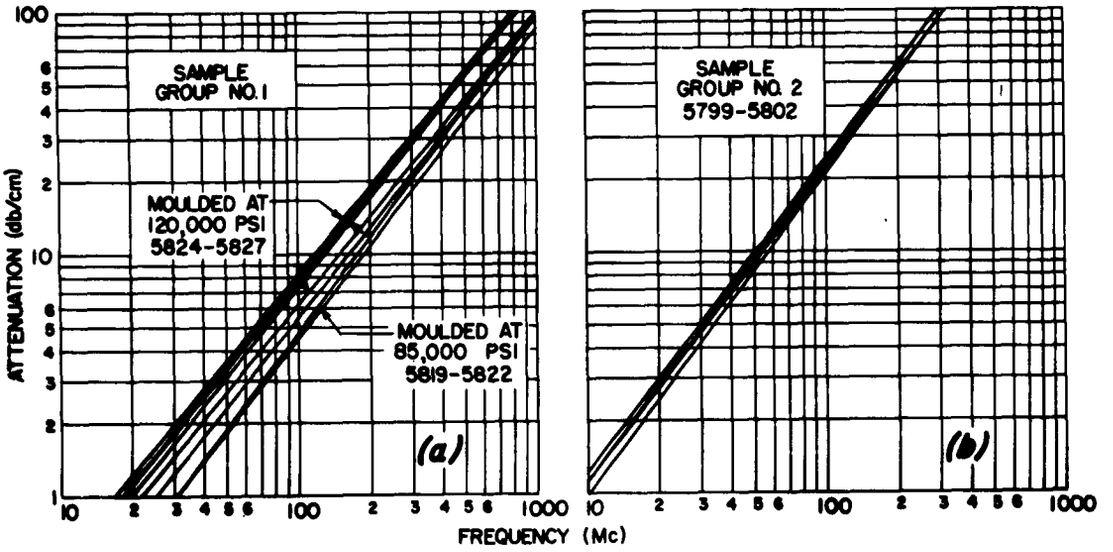

FIG. 2-4. SLOPE LINES FOR SAMPLE LOTS

2.2 Protective Systems

Contributors: Norman P. Faunce and Ernst R. Schneck

2.2.1 Dissipative Filters

Classical electrical filters are quite satisfactory for applications involving the rejection of undesirable frequencies in which the filters' input and output conditions are clearly specified and invariant. There are limitations when the filters' terminations (input and output) are undesignated. In certain cases the network at the filters' input may effect a match with the output terminations, thereby reducing the insertion loss to a very small value, if not to zero. Dissipative filters, on the other hand, are not so easily negated. Because they include dissipative elements, their insertion loss can be made to be relatively high even with input and output conditions adjusted for least loss.

In an effort to obtain 30 db attenuation (dissipative power loss) of RF energy in the frequency range of 20 Kc to 10 Mc, we attempted the design of a dissipative filter. To find what conditions in a network branch give the greatest power dissipation, we first studied elementary circuits that might form a more complex network which would meet design specifications.

A low pass filter is suggested by the response desired, passage of dc and low frequencies essentially unaltered, considerable dissipation of energy at 20 Kc or higher. The frequency-impedance characteristics of inductances and capacitances indicate that they may be used respectively as series and shunt elements in a low pass filter design. These elements will effect an insertion loss which will increase with frequency, but as we will demonstrate, they will not contribute to dissipative power loss.

Consider the circuits shown in Figure 2-5. View (a) shows an inductance, L, in series with a resistive load, R, and view (b) shows a capacitance, C, shunting the load. For our analysis let us define an apparent attenuation (α) as:

$$\alpha = 10 \log_{10} \frac{P_N}{P_R}$$

where P_N represents the power absorbed by the total network and P_R represents that part of the power absorbed solely by the load.

In the case of series RL circuit the apparent input power (P_{in}) is,

$$P_{in} = I^2 Z = I^2 (R + j\omega L) \qquad (2\text{-}4)$$

and the power absorbed by the network will be the real part of this, or

$$P_N = \text{Re}\,(P_{in}) = \text{Re}\left[I^2 (R + j\omega L)\right] = I^2 R \qquad (2\text{-}5)$$

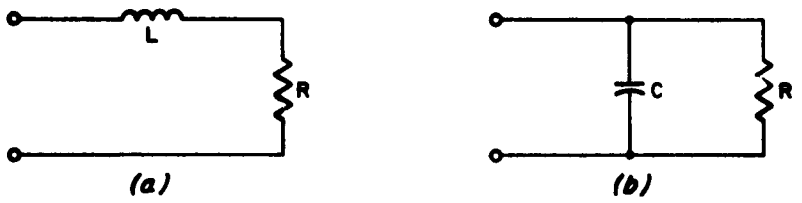

FIG. 2-5. LOSSLESS PRIMITIVE NETWORKS (TYPE I)

The power absorbed by the load, however, is also equal to I^2R, hence the apparrent attenuation is:

$$\alpha = 10 \log_{10} \frac{I^2R}{I^2R} = 0 \tag{2-6}$$

Similarly, for the shunt RC circuit we find by a similar analysis that α is again zero.

We consider now the addition of a resistance to the network in an attempt to make them lossy. Let us consider the addition series-wise, as shown in Figure 2-6.

Adding a loss resistance (r) to the series inductor would increase the apparent attenuation to $10 \log \left(1 + \frac{r}{R}\right)$, but the increased loss is also obtained for dc input.

A series branch containing a resistor and a capacitor shunting the load shows more promise for providing a reasonably lossy branch circuit. The apparent attenuation derived for the network shown in view (b) of Figure 2-6 is given by

$$\alpha = 10 \log_{10} \left[1 + \frac{\omega^2 C^2 Rr}{1 + \omega^2 C^2 r^2} \right] \tag{2-7}$$

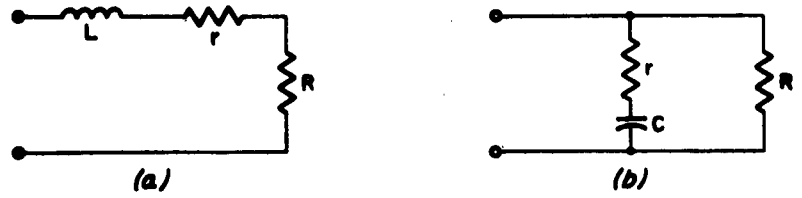

FIG. 2-6. LOSSY PRIMITIVE NETWORKS (TYPE II)

Maximizing this expression with respect to r yields,

$$\alpha_{max} = 10 \log_{10}\left(1 + \frac{\omega CR}{2}\right) \quad , \quad \text{when } r = 1/\omega C. \tag{2-8}$$

To determine how significant this lossy shunt branch might be to a dissipative filter design, we studied it as a protective shunt for a relatively sensitive EED whose bridge resistance is 2 ohms. We arbitrarily designed for 30 db at 100 Kc. From the equation just given, we get C = 1700 pf, and r = 0.001 ohm. Having fixed the component values in this manner, we determined the data of Table 2-15.

Table 2-15

RESPONSE OF RC NETWORK SHUNTING A 2-OHM EED

f (Kc)	P_N/P_R	α' (db)
10	19.76	12.9
20	76.78	18.9
100	1000.	30.0
1000	1981.	32.9

Since the loss below 20 Kc leaves much to be desired, another lossy network might be added to alter the response. Hence, we examined the network shown in Figure 2-7.

The apparent attenuation of this assembly is

$$\alpha = 10 \log_{10}\left[1 + \frac{\omega^2 r L^2 C^2}{R\left[\left(1 - \omega^2 LC\right)^2 + \omega^2 r^2 C^2\right]}\right] \qquad (2\text{-}9)$$

If suitable values are chosen for the parameters in this expression, it can be made to peak at or near 20 Kc, or at any other chosen frequency. For a particular choice of parameter values, a very narrow band resonance response was obtained. It is apparent, however, that combinations of the two previously discussed networks could be analyzed. Because of their complexity, however, it would require undue effort to study the many possible simple combinations; we therefore continued our studies with an analog computer, first investigating the simple network on Figure 2-8.

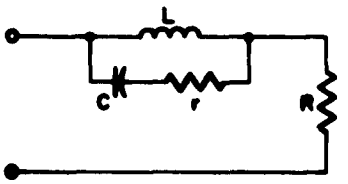

FIG. 2-7. INDUCTANCE WITH LOSSY SHUNT

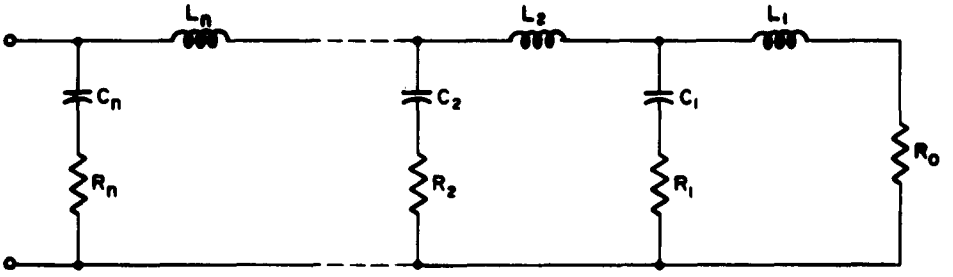

FIG. 2-8. LOSSY NETWORK CONFIGURATION

The terminated power loss ratio (TPLR) for variations of this network has been evaluated over a broad range of frequencies. For this network, if all values of resistance are made equal to $\sqrt{L_n/C_n}$ the network will exhibit a constant impedance independent of excitation frequency. Data has been obtained for this special configuration both as a single loop and as a double loop network (i.e., n = 1 & 2)*. Other data were collected to show the significance of the relative magnitude of the four parameters in the single loop on the frequency dependent loss characteristic.

A network which will present a constant impedance to an energy source independent of the excitation frequency is of interest for many reasons. For example, the design of an energy source is simplified if it is to work into a constant load. For our immediate purpose this special network enables an otherwise complex mathematical expression for TPLR to be reduced to

$$TPLR = \left(1 + Q_L^2\right)^N \qquad (2\text{-}10)$$

where $Q_L = \omega L_N/R_N$; N = number of loops and $\omega = 2\pi f$. The development of this expression was presented in Appendix A of Report P-B1857-7 and it is to a degree verified by the data plotted in Figure 2-9.

Networks of 1, 2.5, and 5.0 ohms constant impedance were evaluated in single loop and double loop configuration to obtain the data of the figure. It may be noted that beyond a frequency of 100 kc the curves are all substantially linear with slopes of 20 db/decade and 40 db/decade for the single and double loop cases respectively. Adding a third loop should increase the slope to 60 db/decade, and a fourth should raise it to 80 db/decade.

---

* It is assumed that $L_1 = L_2 = L_n$ and $C_1 = C_2 = C_n$

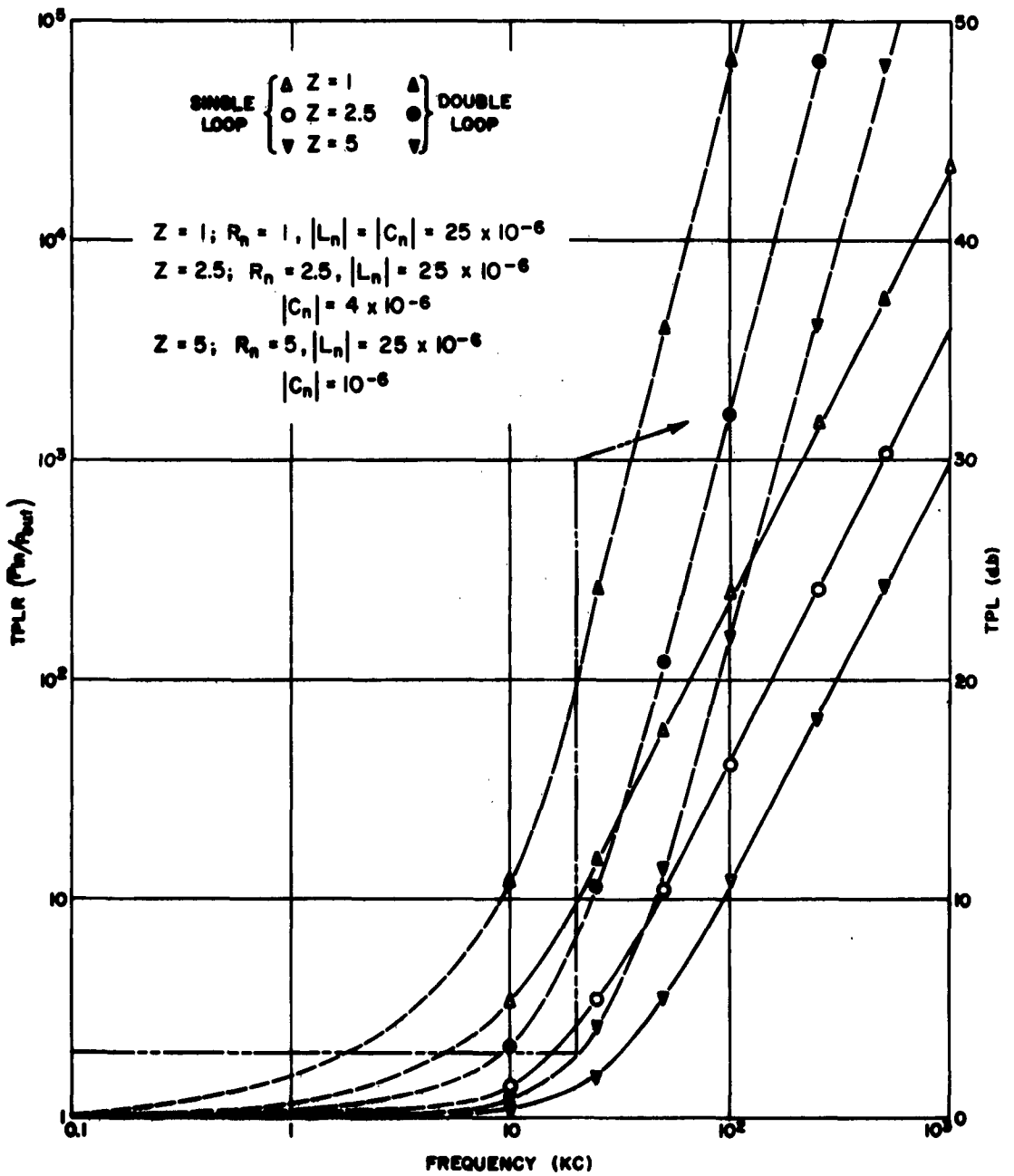

FIG. 2-9. TPLR FOR THREE CONSTANT IMPEDANCE NETWORKS

A further look at these data indicates that the double-loop one-ohm network will provide 20 db of dissipative power loss at 20 kc and that this is increased to 30 db or greater at 35 kc. This same type network, but single loop, would provide only 10 db at 20 kc and does not begin to reach 30 db until a frequency of 200 kc.

Increasing the impedance of the network does little more than to shift the response curve toward the higher frequencies. To obtain loss on the order of 20-30 db at 20 kc for a 2.5 or 5 ohm system would require many loops. The obvious conclusion to be drawn from these data is that we should work with the smallest load possible and increase the number of loops until limited by space considerations or excessive low frequency loss.

If the impedance of the network arrangement shown in Figure 2-8 is to be independent of frequency, a specific relationship must be maintained for the component values. It may be expected that fixing the relative values in this manner will similarly fix the frequency-dependent loss characteristic. However, allowing the parameters to take on other than these ordered values should make some change in the network loss response. To investigate this proposition we computed the TPLR for the single loop network, varying each parameter in turn over a limited range. Results are given in Figure 2-10 through 2-12.

Above a frequency of 100 kc all curves appear to be linear with a slope of 20 db/decade, the same as obtained for the constant impedance networks. Likewise each plot, because of the structure of the network, approaches the asymptote TPLR = 1 as frequency decreases (for d.c., TPLR = 1). The change in slope referred to in the following discussion is the change as we approach this asymptote from the higher frequencies starting at approximately 100 kc.

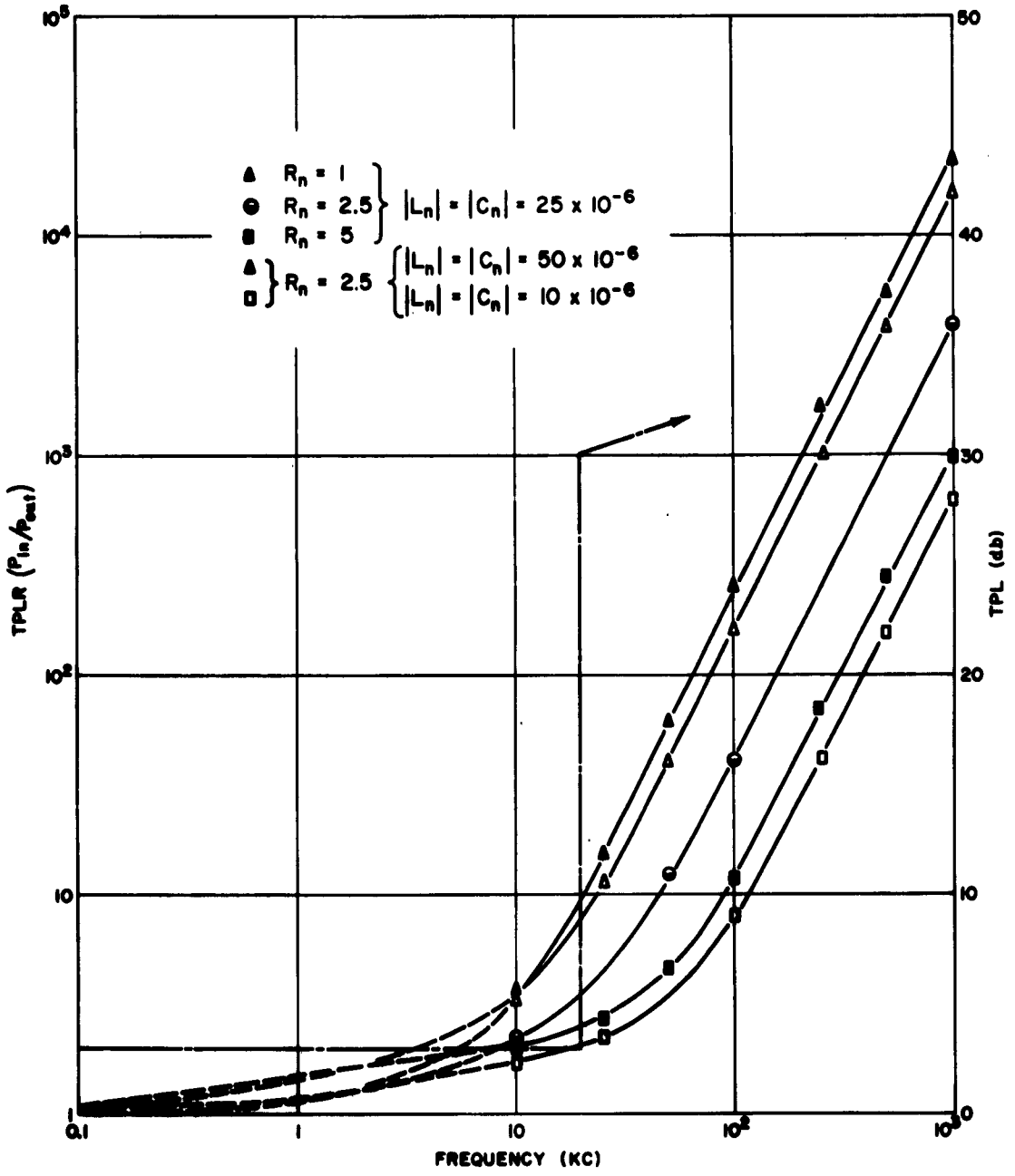

FIG. 2-10. TPLR VARIATION WITH CHANGES IN PAIRED RESISTANCES AND REACTANCES

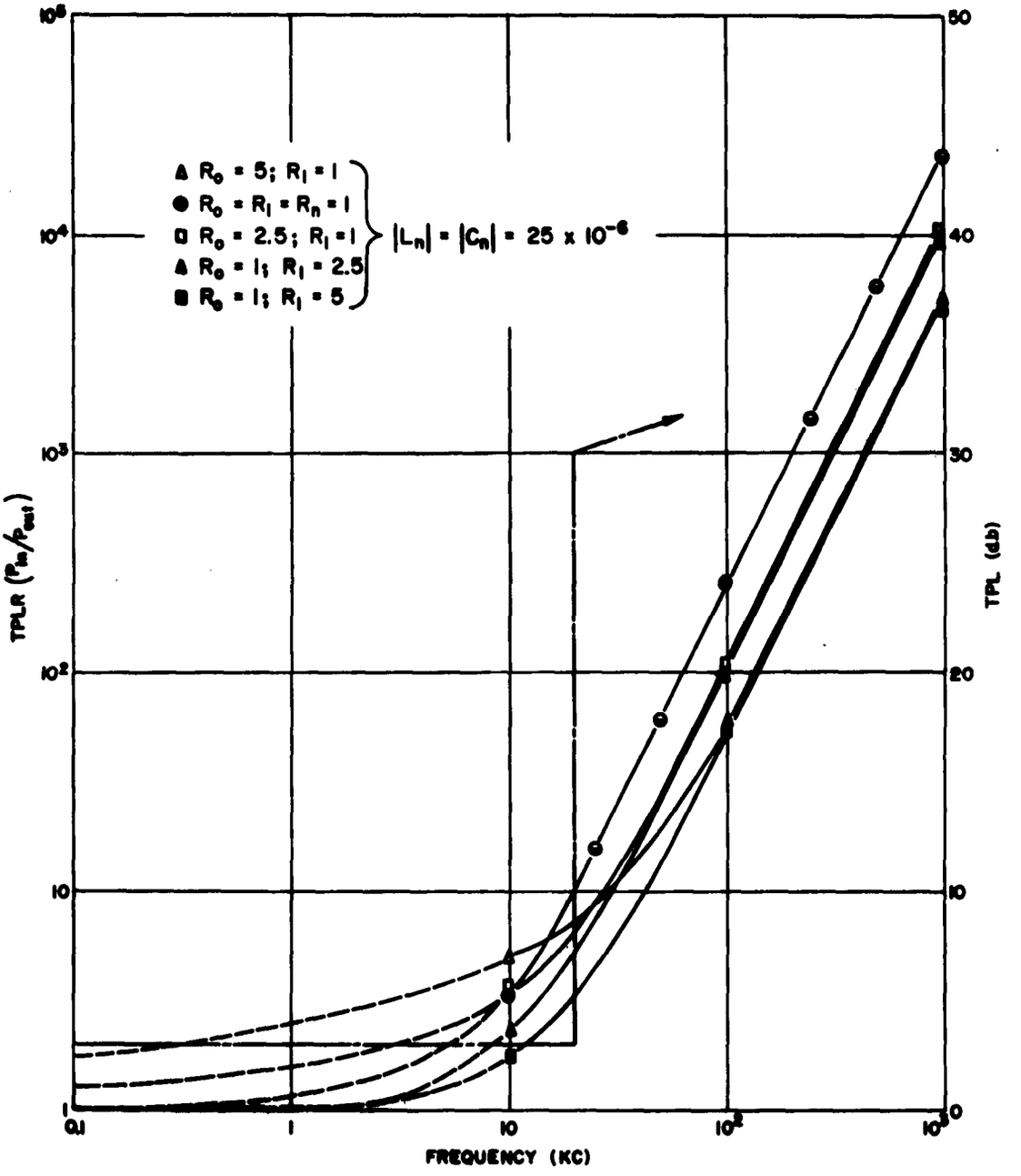

FIG. 2-11. TPLR VARIATION WITH RESISTANCES

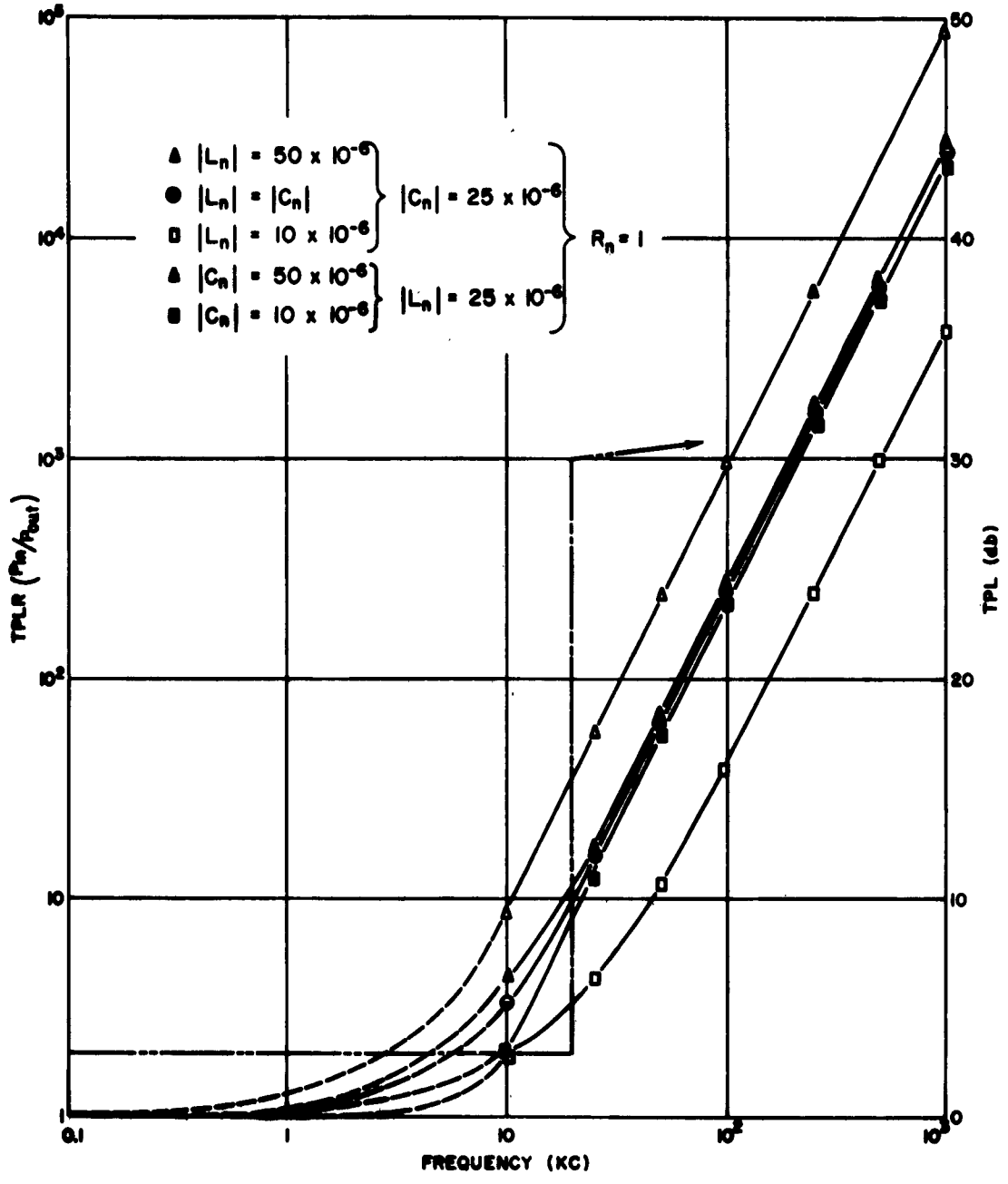

FIG. 2-12. TPLR VARIATION WITH INDUCTANCE AND CAPACITANCE

Figure 2-10 shows the shift in response brought about by allowing the component values to vary in pairs, while maintaining equality of the magnitude of the paired components. R_o was paired with R_1 and L_1 with C_1. The results show that an increase in the value of resistance components brings about a decrease in dissipative loss. Or said another way, this change in parameter values shifts to higher frequency the point at which a specific loss is obtained. These same statements may be made for comparable changes in the values of reactive components, except that increased loss is associated with increased parameter values. In either case, a sevenfold change in parameter value produces a frequency shift of about one decade.

It is of interest to determine how the network loss is modified by changing the resistance values independently. Of special interest is the change brought about by changes in R_o, since this will indicate the range of resistance values of actual EED's that might be protected by one network design. As shown in Figure 2-11, for higher frequencies the response is nearly the same regardless of whether R_o or R_1 is changed.

A more significant change occurs at lower frequencies. With an increase in R_o, as we trace the curve from high to low frequency, the curve begins to flatten out sooner, so that intersection with the curve of lower R_o is observed at a proportionately higher frequency. As we increase R_o, therefore, we increase the losses of the system at low frequency that is, to normal firing pulses. On the other hand, increasing R_1 does not produce this undesirable result; a decrease in loss comparable to that obtained at higher frequencies is also obtained at the lower frequencies.

Finally, we investigated the change in response brought about by changing the inductance and capacitance independently. These results, given in Figure 2-12, show one very interesting result, that changes in the value of capacitance have very little effect on the characteristic system loss. To pursue this study further, we intended to determine the

effect of reducing capacitance to zero. The figure shows us that changing the value of the inductance, however, does give a reasonable change in the loss characteristic, greater loss being associated with higher values of inductance.

Upon digesting the results just presented one might hasten to conclude that a double loop, one-ohm network should provide a very desirable package for a one-ohm EED system. On the basis of the theoretical considerations underlying this study this is a reasonable conjecture. However, the results also show that one might profitably alter the system response by imposing variations in resistance (other than the load), and in inductance, (while adjusting capacitance to any convenient value perhaps equal to zero).

2.2.2 Electroluminescence

The property of interest, common to the ferrites and carbonyl powders, and to dissipative elements, is their ability to convert the energy of an electromagnetic field into another form of energy --- to be specific, heat --- which can be prevented from entering and exciting the critical portion of the electroexplosive device being protected. Another conversion with equivalent effect is afforded by electroluminescent substances, the output being light. It was, of course, within the scope of this project to investigate the potential benefits of such material.

Because zinc sulfide (ZnS) is the most common electroluminescent phosphor, our investigation began with this material. Phosphors generally require activators or substances which when included in the crystals in small quantities stimulate luminescence. Copper is the usual activator for the zinc sulfide crystal, and is usually present in concentrations of roughly 0.01%. Various compounds may carry the copper as CuS, $CuCl_2$, etc. Corresponding to activators, certain substances supress luminescence, and are called "poisons". Since nickel is known to be such a poison to zinc sulfide, the phosphor must be kept strictly free of this element.

There are other factors which influence the efficiency of the electroluminescent process, such as temperature, crystalline properties and grain size. Grain size is known to be related to the amount of energy which phosphor crystal may absorb. Larger grains absorb more energy and should exhibit more efficient luminescence.

Electroluminescence is stimulated by time-varying electric fields impressed across the phosphor. Waveform and amplitude of the signal are major factors determining characteristics of the luminescence. A commonly mentioned relation between luminescent brightness (B) and signal voltage (V) is $B = ae^{-bV}$, where the factors a and b depend upon frequency, temperature, and type of phosphor among others. Certain materials, such as $BaTiO_3$ and ZnO when included in the phosphor preparation, increase the resultant effective dielectric constant. These materials produce a striking non-linear voltage dependence of brightness of the form $B = f(V^n)$, where n may range from 1.5 to approximately 9. The latter relation has been observed for ZnO in ZnS : Cu phosphors, and may be chiefly attributed to dielectric loading, although ZnO does exhibit some electroluminescence, also.

When the electromagnetic field applied to an EL phosphor varies, light is usually emitted. If the frequency of variation increases, the brightness per cycle will be reduced, since the time available for carrier diffusion is shortened. However, a higher signal frequency results in an increased number of light pulses emitted per unit time. These two opposing effects result in a non-linear relation between brightness and frequency. This response exhibits a rise in brightness to a maximum value in the kilocycle frequency region, and a subsequent decay for higher frequencies. Commonly, this may be demonstrated by the maximum brightness exhibited by EL panels for a specific frequency.

Electroluminescent devices, such as EL panels, have complex impedances, varying with both frequency and voltage. Because of the difficulty of expression the impedance in a suitable algebraic form, circuits comprising such components are not easily analyzed.

In an attempt to measure the power absorption of a commercially available ZnS:Cu phosphor we formed the powder into our standard doughnut configuration. The first sample had little mechanical strength and crumbled; we therefore made a second, with a metal band surrounding it. When measured in the coaxial system, we observed no power absorption. A sample formed by a mixture of iron powder and ZnS:Cu showed some power absorption, but this was thought to be due to the iron present.

The most frequent experimental arrangement employs phosphor as a dielectric in a capacitor, the ZnS:Cu being sandwiched between electrodes. Hence, seeking to employ this method, we mixed the EL phosphor with an epoxy adhesive, and formed a capacitor with a dielectric layer 0.02 inch thick. This device had a capacitance of 208 pf at 1 kc and a dissipation factor of 0.11. We concluded that it was not an efficient power absorbing system.

Several factors were thought to impair the power absorption measured with the commercial ZnS:Cu phosphor. They were moisture absorption by the phosphor, small grain size of phosphor used (3.5 microns), low activator concentration (1:3000) and low voltage gradient impressed upon the phosphor particles.

So that we might obtain significant power absorption, we endeavored to produce in our own laboratories, a ZnS:Cu phosphor with ZnO dielectric to induce luminescent activity within a crystal; our production of the material would allow us to control activator concentration and particle size. Manufacture of this material suffered delays due to repeated breakage of the special glass equipment required for firing.

2.2.3 Photoresistive - Electroluminescent Devices

At the beginning of these studies of electroluminescent phenomena we had suggested the use of electroluminescent photo-conductivity (EL-PC) in a radio frequency protective system. Our attention was again drawn to the possibilities existing in this area by their increasingly wide usage in electronic applications.

When photoresistors are exposed to light, their resistance changes. The light could conceivably be supplied by an EL phosphor. These ideas suggest a protective network in which the resistive components are photoresistors, and the excitation is derived from electroluminescent elements used as capacitors in the network. The response of photoresistors changes with the intensity of the incident light and with different wavelengths. Effects of frequency variation and high energy pulses upon photoresistors are not yet well defined. The luminescence of EL phosphors, as noted previously, responds accordingly to various amplitudes, waveforms and frequency of the applied excitation. Consequently, the electrical and optical non-linear characteristics of EL-PC devices might be suitably combined to impart to a circuit specific frequency discriminating characteristics.

Photoresistors, EL panels and PC switches (photoresistor with light source in a single unit) are commercially available. Information regarding the characteristics of primary interest to us, however, is not readily available. For this reason, we obtained several devices and examined them in laboratory tests. Results indicate they have low power handling capabilities and exhibit capacitance coupling in the megacycle frequency range.

In an experiment with separate EL and PC elements, we placed a red EL panel face-to-face with a PC element. The usual PC elements are most sensitive to wavelengths in the red region, hence, the choice of a red EL panel. Various sinusoidal signal frequencies were supplied the EL panel and the corresponding PC resistances noted. Minimal resistances were noted in specific frequency ranges for the various signal voltages applied. Such a result is to be expected since the PC resistance depends upon the integrated luminescence of the EL panel.

Noting that our previous experiment resulted in a minimum resistance of 13 kilohms for the PC element, we sought a means of

obtaining a lower resistance, since this value is far too high for any use we might consider.

Obtaining new elements, which promised superior results, and re-examining them in a similar fashion we obtained data which appeared hopeful. Various EL panels and PC elements were examined for individual variations. The major indications of the experiment were:

(1) The photoresistors tested vary in response; a plot of the group's characteristics (Figure 2-13) form a family of curves.

(2) Their was notable success in reaching a lower minimum resistance; the minimum obtained was less than 250 ohms for 100 volt rms signal, as compared to 13 kilohms previously.

(3) The minimum resistances obtained, if any, generally correspond to higher frequency ranges than in earlier experiments. Previously obtained minimums corresponded to frequencies below 10 kc, while those newly obtained correspond to frequencies above 10 kc; no clear explanation of this is presently available.

We note that in comparison to the previous experiment, a lower PC "on" resistance was obtained. While some improvement was thereby noted, we require a still lower value for practical application. Later examinations of the signal source with an oscilloscope indicated that the probable rms voltage across the EL panels was on the order of 30 volts, and not 100 as indicated.

Various areas are open whereby we might improve the level of response obtained, so as to make it acceptable for application. The first obvious step would be to increase the signal voltage; this would require a signal source able to supply the low impedance panels such stimuli of up to 150 volts rms at frequencies in the kilocycle range. Next one might place several PC elements upon the EL panel (10 or more may fit in our case). This would give sufficient power handling

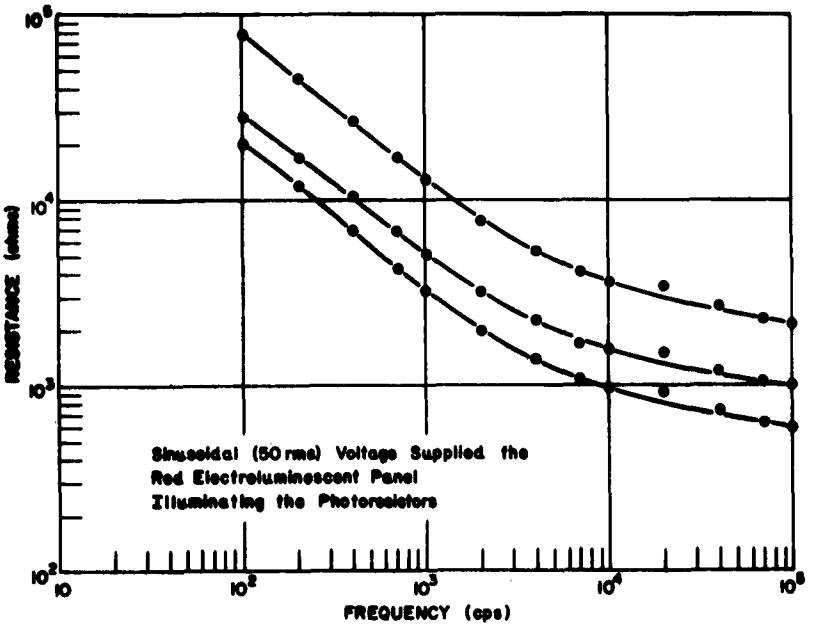

FIG. 2-13. RESISTANCE VERSUS FREQUENCY OF VARIOUS PHOTORESISTORS

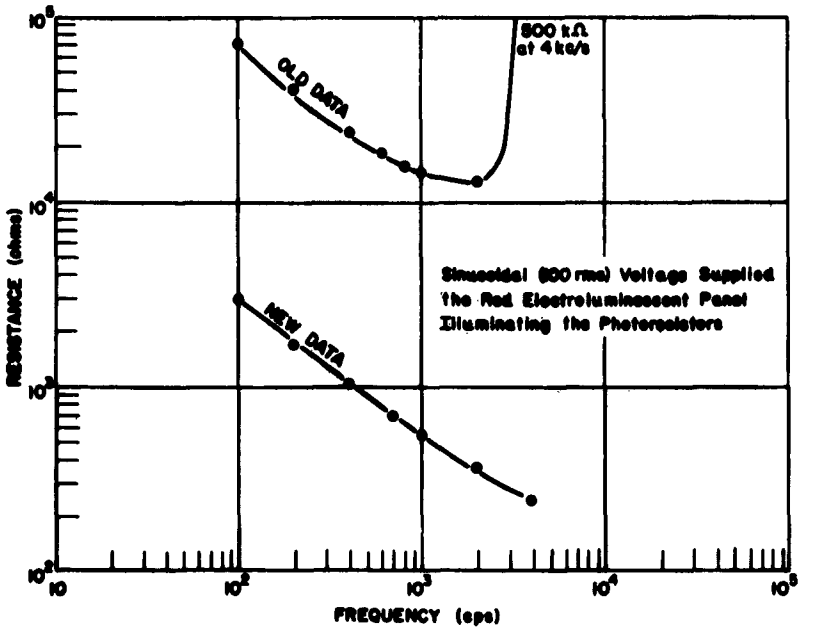

FIG. 2-14. RESISTANCE VERSUS FREQUENCY OF LIGHT DEPENDENT RESISTORS

capabilities, approximately 5 watts, and a lower resistance when the elements are electrically in parallel. Hence, by this method we may improve the formerly inefficient arrangement.

In our case, before we could proceed, we require a transformer to match signal source and EL panel. Due to the anomalous impedance characteristics of the EL elements, variation with respect to voltage and frequency must be determined before a transformer may be described.

2.2.4 Conclusions and Recommendations

Results from EL phosphor studies are relatively scant because of equipment problems. However, the small quantities of data from these studies indicate correspondingly that this material might have limited application to RF hazard protective systems. It would seem advisable, therefore, to cease for the time being, further effort along these lines; we would, however, be alert for promising future developments in this field. Because of the attractiveness of this means for producing light, it is obvious that many new and improved materials will emerge from the research laboratories. As these appear on the market, so will improved means for their characterization be developed. Perhaps within the next two to five years, it may become profitable to re-enter this area of study; for the present, it does not hold any great promise.

On the other hand, it would appear that further work with EL-PC circuitry may be warranted. Results obtained in our studies indicate that a relatively desirable non-linear response is possible with one arrangement of these two elements. Since EL-PC circuits are used in many control operations it would seem that additional study should reveal one or two interesting systems for use as an RF protective device. Since these components are commercially available in many sizes and forms, and with varying response characteristics, a number of unusual circuit arrangements may be examined. It would be advantageous to at least consider their use in some form of arming-type protective systems, for example, one in which the EL-PC circuit is first energized, followed by the firing pulse.

In the realm of dissipative networks a number of interesting schemes seem possible. Networks with input impedance either dependent or independent of frequency can be developed, in theory, to provide high loss. The practicability of resulting network designs is still questionable; that is, though we may specify the magnitude of inductances, capacitances and resistances, they may be impossible to develop in the real physical sense.

With opportunity to use a large scale computer, it is a relatively simple matter to examine the response of a number of relatively complex networks. A further step can be taken; we can examine the peak voltages and currents throughout the system and with those data, completely specify the components required to produce the indicated response. Moreover, the analog approach can be extended to analyses of EL-PC circuits and shielded transformer design. Continuation of this phase of study, enlarged to include the latter, is strongly recommended.

2.3 Evaluation of Ferrites and Other Core-Type Materials

Contributor: Daniel J. Mullen, Jr.

One phase of this project has been especially concerned with evaluation of materials other than carbonyl iron which can be used as attenuators of RF energy. Our success with carbonyl iron resulted in a valuable contribution to the protection of ordnance devices from the hazard of electromagnetic radiation. It is limited in its effectiveness, however, to frequencies of 100 Mc and up. Our experience has indicated that it is possible to obtain interesting values of attenuation at frequencies of 10 Mc - 100 Mc by the use of a class of materials called ferrites. We have already had some experience with these materials having had them under consideration long before we were able to develop a desirable carbonyl iron formulation. Because our first attempt to measure ferrites indicated no consistent noteworthy attenuation at 500 Mc, at least in comparison to the more easily used carbonyl iron formulations, they were set aside for more promising items. It was not until

much later that it was discovered that the particular ferrites that we measured had a skin with high resistance. Removal of the skin enabled us to obtain a value of attenuation which signalled the advisability of further study. Since that time, the study and evaluation of ferrite materials has become a major phase of this project.

Our study is outlined as follows:

1. Material supply
2. Evaluation of samples for attenuating properties
3. Theoretical approach to attenuation
4. Methods of preparation of ferrites

2.3.1 Material Supply

We have been most fortunate in our attempts to secure samples of ferrite toroids for commercial manufacturers. Every manufacturer that we have approached has been very prompt in supplying us with samples. Most of the toroids that we received would not fit our standard holders and we, therefore, had to make special ones. We were able to measure these non-standard samples with our stub matching system but only at frequencies no lower than 150 Mc. One manufacturer, however, supplied us with some samples made to our dimensional specifications, and we were able to measure these samples from over the 10 Mc to 500 Mc range, using the General Radio immittance bridge and our long line system.

In addition to molded samples, we were also given samples of fired ferrite powders for our own fabrication.

2.3.2 Evaluation of Ferrite Materials

After reviewing ferrite literature, we find that there are certain electrical characteristics of the material that are very important in the development of a good attenuator for the low frequencies.

(1) The initial permeability should be high, so that losses due to hysteresis or magnetic resonance may appear at the lowest possible externally applied field [in our case zero field].

(2) The volume resistivity should be as low as permissible in its particular application. This will result in maximum shunt or eddy current losses.

(3) Saturation residual magnetization should be high. The combination of these with high permeability is important. These properties will give a hysteresis loop that is nearly rectangular with the greatest area (largest loss per cycle) for the lowest applied field.

(4) Frequency independence is desirable over a certain range of frequencies. Unless a complex ferrite is developed, the effects of domain wall resonance and ferromagnetic resonance cannot be fully utilized, since these losses peak at certain frequencies.

(5) Temperature stability is desirable because of the wide range of service temperatures.

Information is presented in Table 2-16 showing electrical and magnetic properties of some ferromagnetic materials which are available commercially.

We have received and evaluated samples of ferrites; types T-1, C-27, Q-1 and H-1. A composite plot of attenuation versus frequency is shown in Figure 2-15. This graph shows that of the four, the C-27 ferrite is the best for our purposes. However, the perturbations in the curves for the ferrites do not appear in the carbonyl iron curves. These are probably indicative of resonance and anti-resonance in the ferrite matrix and are related to domain wall rotation, domain resonance, etc. Ferrite development should lessen the degree of perturbation or remove it entirely.

Although we have received a number of different types of ferrites, we have not been able to measure any but the four first mentioned.

Table 2-16

ELECTRICAL AND MAGNETIC PROPERTIES OF FERROMAGNETIC MATERIALS

Name or Type	Initial Perm. 1kc.	1Mc	Max. Perm.	Satur. Flux Dens. (Gauss)	Residual Magn. (Gauss)	Coercive Force (Oersteds)	Volume Resistivity (ohm-cm)	Curie Point (°C)	Dielectric Constant (K)	Manuf. Code
R-02	395	-	810	3000	-	-	1.7×10^6	-	-	106
R-03	325	-	3500	3900	3360	0.37	-	315	-	
WO-1	850	-	5000	2850	-	-	-	-	-	
WO-3	2200	-	6000	4200	-	-	-	-	-	
WO-4	800	-	4700	4600	-	-	-	-	-	
WO-7	1300	-	4000	5200	1000	0.24	-	280	-	
Bx-114	20	-	125	1800	800	8.5	2.5×10^8	250	-	153
Bx-113	75	-	250	2400	1500	5.0	5×10^8	250	-	
CR-80	-	1250	3250	3600	920	0.16	2000	200	-	
CR-70	-	895	2400	4200	1840	0.67	50	210	-	
CR-20	-	210	740	3000	2040	2.5	9×10^6	245	-	
CR-4	-	590	1800	3050	1170	0.5	150	205	-	
CR-S	-	625	1825	4900	2500	1.0	1600	235	-	
101	1100	-	-	2325	1100	0.18	-	100	-	174
102	600	-	-	2500	850	0.4	-	140	-	
103	450	-	-	3500	2400	0.7	-	265	-	
104	200	-	-	3400	2575	2.1	-	385	-	
105	95	-	-	3030	2025	4.2	-	465	-	
106	30	-	-	2000	1300	11.2	-	585	-	
3	1000	-	-	3400	-	-	-	130	-	
3A	1400	-	-	3100	-	-	20	212	-	
3B	900	-	-	3900	-	-	20	300	-	
3C	900	-	-	3700	-	-	-	170	-	
B2	900	-	-	3900	-	-	80	300	-	
B3	900	-	-	3900	-	-	120	300	-	
3C2	1100	-	2000	3800	-	-	80	300	-	
3D2	750	-	1600	3900	-	-	80	410	-	
4A	600	-	-	3200	-	-	1×10^5	255	-	
4B	250	-	750	3700	-	-	1×10^8	480	-	
4C	125	-	-	3400	-	-	1×10^8	660	-	
4D	50	-	-	3000	-	-	1×10^5	750	-	
4E	15	-	-	2100	-	-	1×10^5	930	-	

Table 2-16 (continued)

ELECTRICAL AND MAGNETIC PROPERTIES OF FERROMAGNETIC MATERIALS

Name or Type	Initial Perm. 1kc	1Mc	Max. Perm.	Satur. Flux Dens. (Gauss)	Residual Magn. (Gauss)	Coercive Force (Oersteds)	Volume Resistivity (ohm-cm)	Curie Point (°C)	Dielectric Constant (K)	Manuf. Code
O-1	-	800	4200	4200	1600	0.24	Low	190	-	190
O-2	-	1100	3100	4500	1600	0.30	Low	190	-	
O-3	-	1500	4000	4500	1600	0.15	Low	190	-	
Q-1	-	125	400	3300	1800	2.1	High	350	-	
H-1	-	550	3800	2800	1500	0.35	Med.	125	-	190
H-3	-	550	3800	2800	1500	0.35	High	125	-	
T-1	-	2000	3600	4400	1000	0.18	Low	180	-	
C	-	250	1100	4200	2700	2.1	-	330	-	
D	-	410	1030	3100	1320	1.0	-	160	-	
E	-	750	1710	3800	1950	0.65	-	160	-	
G	-	410	3300	3200	1050	0.25	-	160	-	
H	-	850	4300	3400	1470	0.18	-	160	-	
I	-	900	3000	2000	700	0.3	-	70	-	
M	-	200	500	3000	2300	0.5	-	290	-	
A	25	-	100	2000	1500	5.6	-	-	10	
B	100	-	167	1900	900	2.5	-	-	6000	
C[1]	900	-	1000	3600	2800	1.5	-	-	10000	
D[1]	600	-	1200	2960	2000	0.8	-	-	20000	
E[1]	660	-	940	3360	1600	0.75	-	-	200	
G[1]	1670	-	1860	3200	1200	0.25	-	-	10	
F[1]	1670	-	3000	3200	1200	0.2	Med.	-	1000	
H-1[1]	1250	-	3750	2960	1600	0.18	Med.	-	7000	
J	400	-	800	2960	2000	1.2	-	-	11	
Q	167	-	400	3320	1200	1.5	High	-	11	
MF 874	225	-	600	3320	2240	1.6	-	-	80	
1326B	125	-	600	1900	1650	1.4	-	-	10	
1331	90	-	378	1600	1300	1.8	-	-	11	
R-1	-	45	320	1760	1240	2.1	-	290	-	
R-4	-	40	470	1780	1490	1.4	-	320	-	
R-5	-	65	420	1110	790	0.8	-	140	-	
R-6	-	70	480	730	490	0.7	-	100	-	

Table 2-16 (continued)

ELECTRICAL AND MAGNETIC PROPERTIES OF
FERROMAGNETIC MATERIALS

Name or Type	Initial Perm. 1kc	Initial Perm. 1Mc	Max. Perm.	Satur. Flux Dens. (Gauss)	Residual Magn. (Gauss)	Coercive Force (Oersteds)	Volume Resistivity (ohm-cm)	Curie Point (°C)	Dielectric Constant (K)	Manuf. Code
O-1	-	800	4200	4200	1600	0.24	Low	190	-	190
O-2	-	1100	3100	4500	1600	0.30	Low	190	-	
O-3	-	1500	4000	4500	1600	0.15	Low	190	-	
Q-1	-	125	400	3300	1800	2.1	High	350	-	
H-1	-	550	3800	2800	1500	0.35	Med.	125	-	190
H-3	-	550	3800	2800	1500	0.35	High	125	-	
T-1	-	2000	3600	4400	1000	0.18	Low	180	-	
C	-	250	1100	4200	2700	2.1	-	330	-	
D	-	410	1030	3100	1320	1.0	-	160	-	
E	-	750	1710	3800	1950	0.65	-	160	-	
G	-	410	3300	3200	1050	0.25	-	160	-	
H	-	850	4300	3400	1470	0.18	-	160	-	
I	-	900	3000	2000	700	0.3	-	70	-	
M	-	200	500	3000	2300	0.5	-	290	-	
A	25	-	100	2000	1500	5.6	-	-	10	
B	100	-	167	1900	900	2.5	-	-	6000	
C[1]	500	-	1000	3600	2800	1.5	-	-	10000	
D[1]	600	-	1200	2960	2000	0.8	-	-	20000	
E[1]	660	-	940	3360	1600	0.75	-	-	200	
G[1]	1670	-	1860	3200	1200	0.25	-	-	10	
H[1]	1670	-	3000	3200	1200	0.2	Med.	-	1000	
H-1[1]	1250	-	3750	2960	1600	0.18	Med.	-	7000	
J	400	-	800	2960	2000	1.2	-	-	11	
Q	167	-	400	3320	1200	1.5	High	-	11	
MF 874	225	-	600	3320	2240	1.6	-	-	80	
1326B	125	-	600	1900	1650	1.4	-	-	10	
1331	90	-	378	1600	1300	1.8	-	-	11	
R-1	-	45	320	1760	1240	2.1	-	290	-	
R-4	-	40	470	1780	1490	1.4	-	320	-	
R-5	-	65	420	1110	790	0.8	-	140	-	
R-6	-	70	480	730	490	0.7	-	100	-	

Table 2-16 (continued)

ELECTRICAL AND MAGNETIC PROPERTIES OF FERROMAGNETIC MATERIALS

Name or Type	Initial Perm. 1kc	1Mc	Max. Perm.	Satur. Flux Dens. (Gauss)	Residual Magn. (Gauss)	Coercive Force (Oersteds)	Volume Resistivity (ohm-cm)	Curie Point (°C)	Dielectric Constant (K)	Manuf. Code
5N	480	-	1530	2500	1250	0.55	1.2×10^{3}	200	4.4×10^{4}	272
7A	780	-	4700	2800	2150	0.35	5×10^{8}	175	8.0×10^{3}	
9	190	-	490	3000	1980	2.0	1×10^{11}	210	-	
20	1835	-	5550	3950	1550	0.19	2.3×10^{4}	169	3.4×10^{3}	
23	1200	-	4000	3400	1750	0.33	5×10^{3}	158	4.35×10^{4}	
23B	420	-	1880	3950	2200	0.72	270	610	-	
27	920	-	2390	4200	1925	0.5	2.2×10^{3}	224	8.0×10^{4}	
1848	160	-	300	2600	1650	2.9	-	220	-	
2285	133	-	38	2100	1600	21	5.5×10^{9}	510	10.5	
11	115	-	307	2540	1420	2.8	2.5×10^{7}	385	-	272
25	500	-	-	-	-	-	-	156	-	
25A	600	-	-	-	-	-	-	156	-	
F-45	-	650	4000	3900	-	0.18	10^{7}	150	-	340
F-6-18	-	6	80	300	250	20	7×10^{7}	200	-	
F-6-23	-	13	125	600	500	20	7×10^{7}	200	-	
F-7B	-	300	750	2900	1600	0.80	7×10^{7}	200	-	
F-15	-	300	1500	5000	3000	0.80	10^{7}	200	-	
F-27S	-	1050	2800-3500	2500-2800	800	0.18	5×10^{7}	117-127	-	
F-35	-	300	930	2800	-	0.80	10^{7}	200	-	
F-62S	-	300	3500	2900	1400	0.18	10^{7}	117-127	-	
F-73	-	437	4000-5000	4400-4550	1500	0.20	10^{8}	150	-	
F-112	-	1000	1800	3400	700	0.25	100	130	-	
F-200	-	145	450	3000	1400	2.0	10^{7}	300	-	
84	-	142	3200	3155	1226	0.296	-	370	-	662
MB	-	1550	4400	4200	1700	0.42	-	230	-	
MC	-	480	1600	2700	1040	0.52	-	215	-	
CQ	10	100	-	1000-3000	-	2-10	-	350	-	

Table 2-16 (continued)

ELECTRICAL AND MAGNETIC PROPERTIES OF FERROMAGNETIC MATERIALS

Name or Type	Initial Perm. 1kc	1Mc	Max. Perm.	Satur. Flux Dens. (Gauss)	Residual Magn. (Gauss)	Coercive Force (Oersteds)	Volume Resistivity (ohm-cm)	Curie Point (°C)	Dielectric Constant (K)	Manuf. Code
1	3	-	40	2560	2080	6	-	-	20 (IMC)	M.I.T.
2	100	-	660	2700	2200	1.8	-	-	10^4 "	|
3	40	-	270	1700	1300	1.9	-	-	10^8 "	|
4	50	-	130	875	600	1.8	-	-	10 "	|
5	50	-	125	1850	750	3.25	-	-	300 "	|
6	100	-	260	2600	1100	2.5	-	-	700 "	|
7	200	-	500	3500	1500	1.8	-	-	2000 "	|
8	500	-	800	3900	1700	1.0	-	-	150 "	|
9	480	-	1100	4100	1500	0.7	-	-	400 "	|
10	600	-	1400	3500	500	0.3	-	-	4000 "	|
11	400	-	2000	4000	1500	0.5	-	-	2500 "	|
12	800	-	6000	2700	500	0.13	-	-	3000 "	|

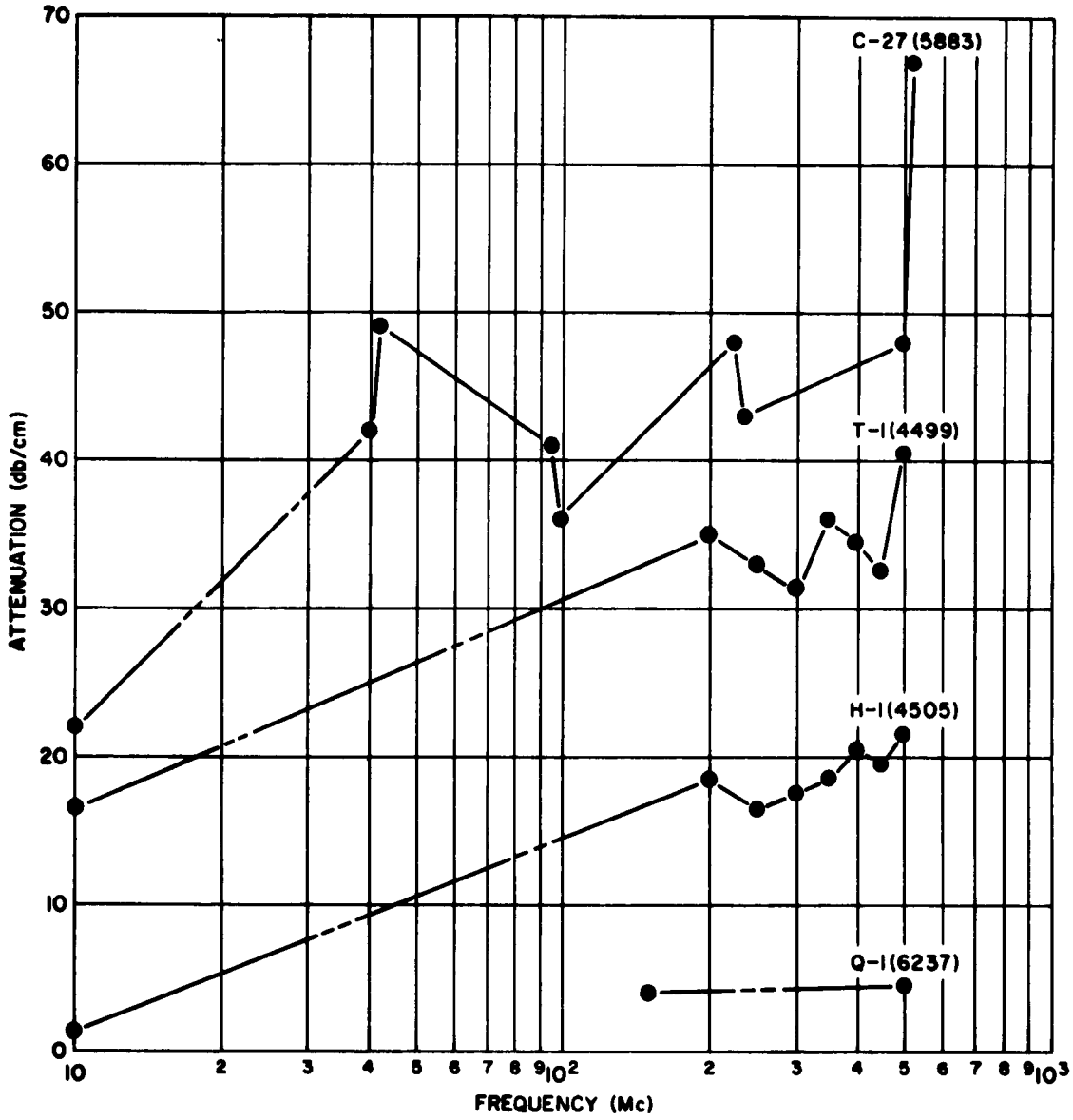

FIG. 2-15. ATTENUATION MEASUREMENTS OF FERRITE MATERIALS

This has been brought about by the variations in dimension of the toroids which we could not accommodate in our sample holders. Several experimental holders were designed but were not successful. Efforts to correlate measurements made on our standard-sized samples with those made on commercial toroids were not conclusive.

It remained, therefore, that the only samples which gave fairly reproducible data were those made especially for us. Future evaluation of other types will require molding our own or having the samples manufactured to our specification.

2.3.3 Theoretical Approach to Attenuation

Our ultimate aim is to be able to specify the parameters that will maximize attenuation. To aid in this, an equation was developed that relates attenuation to frequency, permittivity, permeability, and loss tangents. This equation can be written as follows:

$$\alpha = 128 \times 10^{-11} f \left\{ k'_\epsilon k'_\mu \left((\tan \delta_\epsilon \tan \delta_\mu - 1) + \sqrt{1 + \tan \delta_\epsilon{}^2 \tan \delta_\mu{}^2 + \tan \delta_\epsilon{}^2 + \tan \delta_\mu{}^2} \right) \right\}^{1/2} \qquad (2\text{-}11)$$

where α, the attenuation in db per centimeter is given as a function of f, the frequency in cycles per second,

k'_ϵ = permittivity relative to free space

k'_μ = permeability relative to free space

$\tan \delta_\mu$ = magnetic loss tangent

$\tan \delta_\epsilon$ = dielectric loss tangent

To clarify relationships and to enable us to look for specific values of these parameters, two graphs (Figures 2-16 and 2-17 were plotted. These show the relationship of attenuation to frequency, with the product of the real parts of complex relative permeability and complex relative permeability and complex relative permittivity as parameters with different values of loss tangent assumed.

Of course, each one of these parameters is frequency dependent, and therefore the use of these graphs is limited. They serve, however, to suggest the proper parameters to obtain a certain attenuation, say 30 db, at a particular frequency. It would remain to develop a ferrite that combines these various parameters to obtain a working model.

In Section 2.3.2, it was mentioned that high initial permeability and low volume resistivity should be looked for in the choice of ferrites for use as attenuators of RF energy at low frequencies. We have listed these properties for various powdered materials in Table 2-17 and Table 2-18 beginning with the lowest values and ascending to the highest. The tables are to aid in making a choice of ferrite for further evaluation.

Unfortunately, this aspect of the study was not pursued because of difficulties in securing samples and also because of the lack of time. However, some preliminary data indicates that the theory has merit and should not be left unresolved.

2.3.4 Methods of Preparing Ferrites

Ferrites are prepared by a ceramic technique which involves sintering the component oxides at temperatures between 1000°C and 1450°C. The stages in the preparation of ferrites are listed below:

1. Raw material
2. Decomposition to oxide
3. Milling
4. Presintering (partial reaction)
5. Remilling

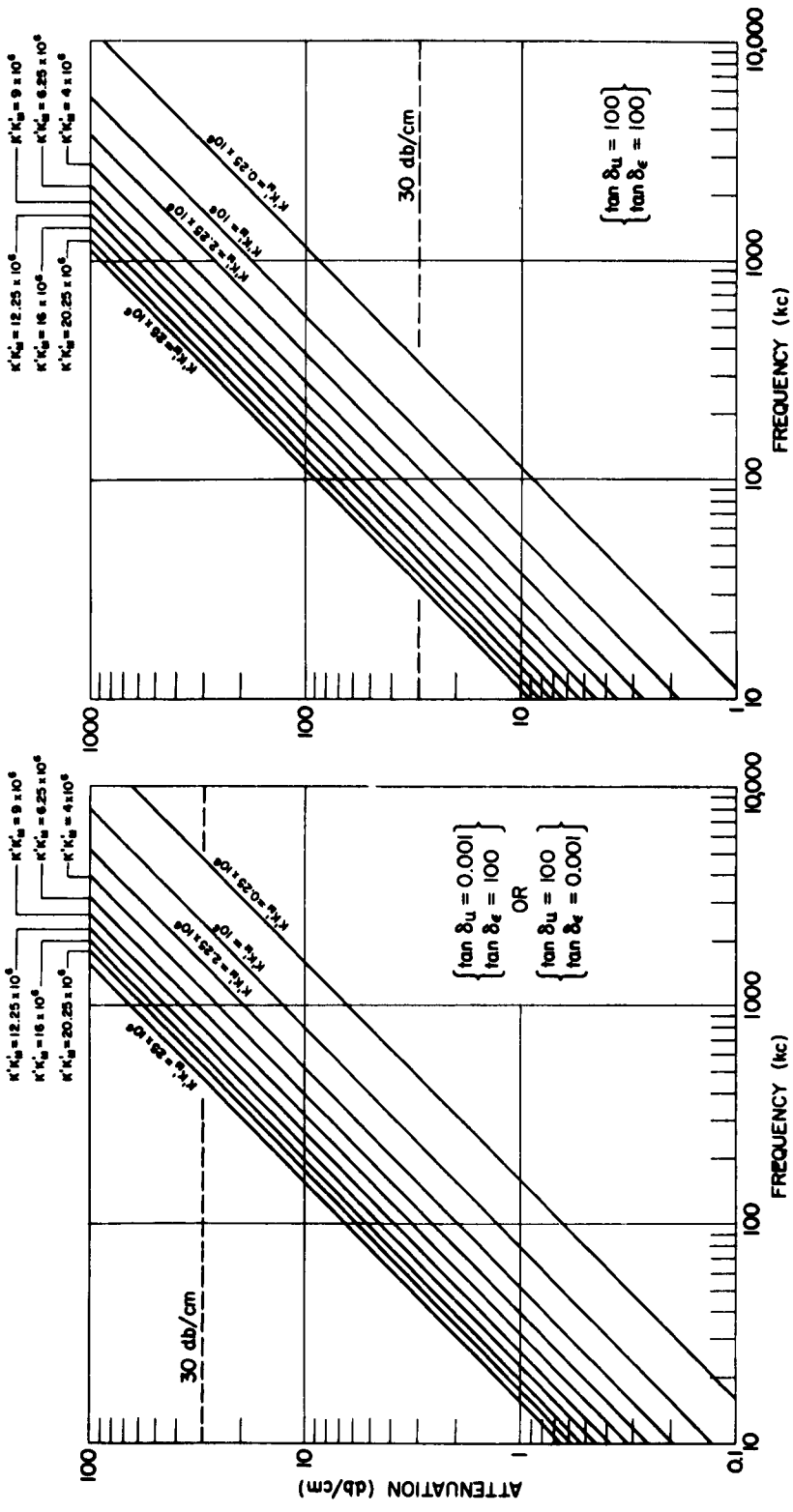

FIG. 2-16. ATTENUATION VERSUS FREQUENCY
(High and Low Values of Loss Tangents)

FIG. 2-17. ATTENUATION VERSUS FREQUENCY
(Loss Tangent, Both Values High)

Table 2-17

POWDERED MATERIALS
INITIAL PERMEABILITY (1 MC)

Name or Type	Initial Perm (1 Mc)	Manuf. Code
F-6-18	6	340
F-6-23	13	340
Q-2	40	190
R-4	40	190
R-1	45	190
R-5	65	190
R-6	70	190
CQ	100	662
Q-1	125	190
84	142	662
F-200	145	340
N	200	190
CR-20	210	153
C	250	190
F-7B	300	340
F-15S	300	340
F-35	300	340
F-62S	300	340
D	410	190
G	410	190
F-73	437	340
MC	480	662
H-1	550	190
H-3	550	190
CR-4	590	153
CR-S	625	153
F-4S	650	340
E	750	190
O-1	800	190
H	850	190
CR-70	895	153
I	900	190
F-112	1000	340
F-27S	1050	340
O-2	1100	190
CR-80	1250	153
O-3	1500 at 100 kc	190
MB	1550	662
T-1	2000 at 100 kc	190

Table 2-18

POWERED MATERIALS
VOLUME RESISTIVITY (OHM-CM)

Name or Type	Vol-Res. (ohm-cm)	Manuf. Code
O-1	Low	190
O-2	Low	190
O-3	Low	190
T-1	Low	190
3A	20	174
3B	20	174
CR-70	50	153
3C2	80	174
3D2	80	174
B2	80	174
F-112	100	340
B3	120	174
CR-4	150	153
23B	270	272
5N	1200	272
CR-S	1600	153
CR-80	2000	153
27	2200	272
H-1	Med	190
Ferramic H	Med	190
Ferramic H1	Med	190
7A	5000	272
23	5000	272
20	23000	272
F-73	100,000	340
4A	100,000	174
4B	100,000	174
4C	100,000	174
4D	100,000	174
4E	100,000	174
R-02	1.7×10^6	106
Bx-114	2.5×10^6	153
CR-20	9×10^6	153
F-4S	10^7	340
F-15S	10^7	340
F-35	10^7	340
F-62S	10^7	340
F-200	10^7	340
11	2.5×10^7	272
F-27S	5×10^7	340
Bx-113	5×10^7	153
F-6-18	7×10^7	340
F-6-23	7×10^7	340
F-7B	7×10^7	340
2285	5.5×10^9	272
9	10^{11}	272
H3	High	190
Q-1	High	190
Ferramic Q	High	190
Q-2	High	106

6. Pressing
7. Final sintering
8. Grinding to shape

A number of raw materials can be used in the manufacture of ferrites; these include oxides, carbonates, oxylates and nitrates. The last three compounds decompose to oxides on heat treatment and are therefore prepared at a temperature at which solid state reactions begin. This process favors a formation of good quality homogeneous materials.

Raw materials are first milled, usually in a steel ball mill to make a homogeneous mixture of very fine particles. The process is carried out with the raw materials in a slurry, using methylated spirit or any other liquid which is easily removed after milling. The mixture of raw materials is then prefired at a temperature about 200°C below its final firing temperature. This process causes partial reaction of the constituents and helps to reduce shrinkage during final sintering. The presintered material is remilled and then, after adding a small quantity of binder (distilled water), the powder is die-pressed to shape, using a molding pressure of 2-10 tons per square inch. After molding, the sample is heated slowly to remove the binder. Slow heating is necessary to avoid cracking of the sample.

The properties of the final product depend critically on the sintering process, and the closest control of sintering time, temperature and atmosphere is required. Generally, sintering is carried out at a temperature between 1000°C and 1450°C for between 4 hours and 24 hours, depending on the ferrite. Ferrites containing nickel, cobalt, or magnesium are sintered at the highest temperatures.

Unless great care is taken in the manufacture, the final ferrite formed is not exactly that corresponding to the proportions of the raw materials used. This is because most ferrites can take up oxides into solution without forming a second phase and therefore

give rise to a non-stoichiometric mixture. During sintering, there is a tendency for most ferrites to give off oxygen, since the equilibrium pressure in this reaction is often greater than one atmosphere and increases rapidly with temperature. This gives rise to an oxygen deficiency in the final product and to the formation of ferrous ions. Here is one phenomenon that might be utilized in the manufacture of a very lossy ferrite, for the presence of ferrous ions in microwave ferrites causes increased dielectric and magnetic losses.

Another problem in final sintering is shrinkage, which may be controlled by careful preparation and by uniform heating of the sample.

Initial production of attenuators from fired ferrite powders were not very successful because of poor mechanical strength. To overcome this, we have added binders in varying percentages. These have improved sample strength somewhat but not to any great extent. The attenuation measurements varied from 2.5 db per sample to 5 db per sample and the dc resistance varied from 500 ohms to 10,000 ohms. These experiments led us to conclude that sintering would probably be necessary to achieve the sought for mechanical strength. However, we still had the problem of crumbling, when no binder was used. We decided to try etching the powder to improve its cohesion when pressed into a toroid configuration. The powder was immersed in a solution of 5% HNO_3 for two hours, then washed with distilled water and dried in an oven at 130°C. These samples were strong enough to hold up under the sintering procedure.

The use of water as a binder was of some help in molding ferrite powders. Water was used because it will evaporate during the sintering operation and leave no residual contaminants. One drop of water per sample was found to be sufficient to enable us to sinter it. The water-bound samples were placed in an oven at 500°F for five or six hours. The treatment improved the mechanical strength of our samples, but attenuation was uneffected.

The next step was to try total sintering of the samples at 2000°F for four hours. This operation gave us good mechanical strength; the attenuation of these samples was, however, adversely affected. The attenuation in all cases was less than 3 db/cm at 500 Mc but the dc resistance increased to well over 2 megohms. Up to this time, our efforts to fabricate ferrites without total sintering and controlled atmospheres have not been successful, but further work is undoubtedly warranted.

2.4 Transverse Magnetic Propagation in a Special Case Coaxial System

Contributor: Ramie H. Thompson

The general problem of predicting attenuation from physical transmission line parameters when the line is constructed of good conductors is well covered in the literature.[1,2] Almost all the effort toward developing attenuation by specification of material parameters has been made with the tacit assumption that the line itself will be of good conducting material and the attenuating material will be inserted in some manner between these good conductors. This assumption made available for use the considerable body of knowledge in the literature. Even here, however, there are some limitations. These assumptions, if the limitations listed in reference 3 below are satisfied, insure the validity of the conventional transmission line equations.

Qualitatively we may say that the question of the validity of the conventional transmission line equations is one of mode of propagation. If the propagating mode is TEM, then the transmission line equations

---

[1] Ramo and Whinnery, Fields and Waves in Modern Radio (New York: John Wiley and Sons, Inc., 1953).

[2] J. A. Stratton, Electromagnetic Theory (New York: McGraw Hill Book Co., Inc., 1941).

[3] Ramo and Whinnery, op. cit. p. 343-344.

hold. It can be shown that inside a closed structure no purely TEM propagating wave can exist; however, under the conventional transmission line assumptions the mode is so close to TEM that there is very little quantitative difference between TEM results and actual observed quantities. In sum, the further we depart from TEM propagation the less we can trust the results of conventional transmission line theory.

In practice, it seems that obtaining a high attenuation constant at low frequency involves specification of parameters for the attenuating material that are not at present physically obtainable. Our chief hope in obtaining material with the correct physical parameters is by a thorough investigation of the ferrites now available. These materials will, of course, have to conform to the validity conditions of the transmission line equations, since the predicted attenuation is based on these equations.

Another approach to obtaining high attenuation at low frequencies is to ignore the approximations necessary for TEM propagation and solve the general case propagation problem. In our particular case, we would like to solve the coaxial line configuration since it has an outer conductor that behaves as a grounded shield. The general case has been treated[4] without considering a magnetic loss term; the results require specification of at least one more quantity than is given and therefore we cannot solve for the propagation constant. (Even if this other quantity were given, the equation would still be a complex transcendental and contain both Bessel and Neuman functions). If the assumption is made that the material between inner and outer conductors is very thin compared to its radius, and that the skin depth of the outer medium is small in comparison to this radius then the problem reduces to finding the propagation constant in the system diagrammed in Figure 2-18.

---

[4]Stratton, op. cit. p. 545-548.

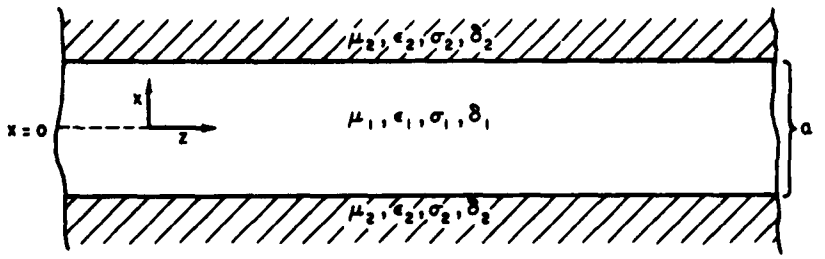

FIG. 2-18. SECTION OF INFINITE PLANE TRANSMISSION SYSTEM

FIL Report P-B1857-10, from which this material is drawn, shows that this configuration is equivalent to that shown in Figure 2-19, as far as propagation of TM waves are concerned.

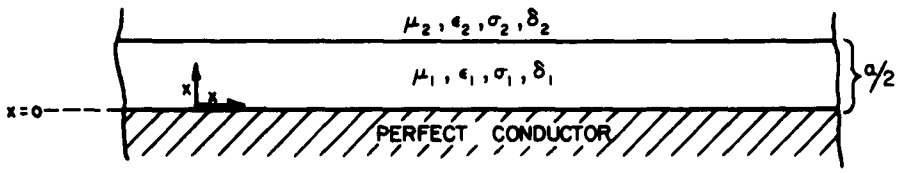

FIG. 2-19. A CONFIGURATION EQUIVALENT TO FIG. 2-18. FOR TM WAVES

Our composite model can now be drawn as Figure 2-20. The assumptions here are that r >> a and that the skin depth in medium 2 is much less than r.

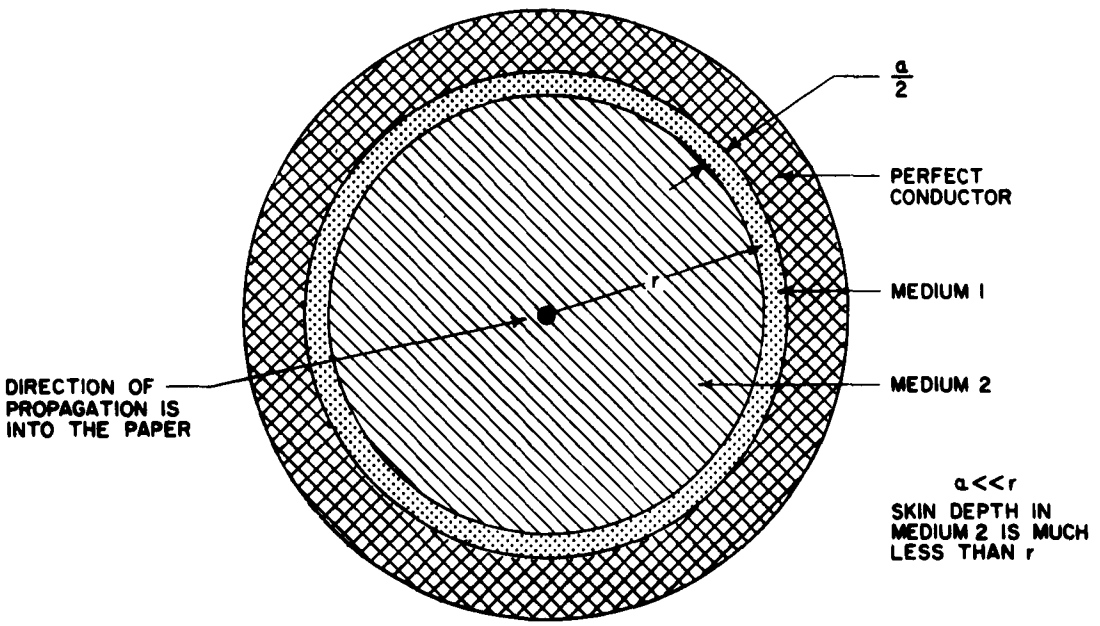

FIG. 2-20. CROSS-SECTION OF SPECIAL COAXIAL MODEL

The equation which determines the propagation constant of TEM waves in the system of Figure 2-20 was found to be

$$\frac{-j\omega\epsilon_1^*}{K_1}\cos\left(K_1\, a/2\right) + \frac{\omega\epsilon_2^*}{K_2}\sin\left(K_1\, a/2\right) = 0 \qquad (2\text{-}12)$$

where $K_1 = \pm\sqrt{\gamma^2 + \mu_1^*\,\epsilon_1^*\,\omega^2}$

$K_2 = \sqrt{\gamma^2 + \mu_2^*\,\epsilon_2^*\,\omega^2}$ [Choose the root which has a negative imaginary part]

$\gamma = \alpha + j\beta$ = propagation constant

μ_1^* = complex permeability of medium 1

ϵ_1^* = complex permittivity of medium 1

μ_2^* = complex permeability of medium 2

ϵ_2^* = complex permittivity of medium 2

$\omega = 2\pi x$ frequency

The roots of Eq. 2-12 define the desired propagation constants. Since Eq. 2-12 is a complex transcendental equation, no explicit solution of the roots may be written. A computer program was written to obtain these roots, but due to limited memory space the program cannot consider complex permeabilities.

We have obtained two solutions from the program to date. Referring to Figure 2-19, the constants were:

$\omega = 2\pi \times 10^6$

$\mu_{1r} = 2000$

$\epsilon_{2r} = 10$

$\sigma_2 = 100$ ohms/meter - conductivity of medium 2

$\mu_{1r} = 1$

$\epsilon_{1r} = 5000$

$\sigma_1 = 0$ - conductivity of medium 1

$a/2 = 1 \times 10^{-3}$ inches - first run

$a/2 = 0.5 \times 10^{-3}$ inches - second run

where the r subscript denotes value relative to free space.

The first run (a/2 = 1 mil) gave an attenuation constant of 12.5 db/cm, the second run (a/2 = 0.5 mils), 18 db/cm. The problem of determining which mode these results represent is still under study. As a measure of the accuracy of the machine program, the two terms of Eq. 2-12 were examined at the root. For the a/2 = 1 mil case, the real parts agreed to 0.25%, the imaginary parts to 0.95%. For the a/2 = 0.5 mil case, the real parts agreed to 0.04%, and the imaginary to 0.19%.

3. CHEMICAL STUDY

During the first part of the project, we tried to improve the RF parameters, attenuation, resistance, and voltage breakdown of samples made with carbonyl iron. The two major phases investigated were effect of particle size and effect of various coatings. At the same time, we did a cursory investigation of nickel, zinc, sponged iron and alnico powders to compare their properties with those of carbonyl iron.

3.1 Particle Size Study of Carbonyl Iron

The particle size of carbonyl iron powder given by the manufacturer is an average value. The particles are distributed around the mean within a reasonably well-defined range. Figure 3-1 gives an example of the distribution for the 10-micron carbonyl iron powder.

Our "standard" attenuator is made from carbonyl iron powder of 10-micron average particle diameter. This size was chosen early in the development of powdered iron attenuators because it was the easiest to insulate and gave the most consistently reproducible results when coated by the old water-phosphate system.

Since that time, we have switched to an acetone-phosphate system which utilizes acetone in place of water. We did this because it keeps oxidation of the carbonyl iron powder to a minimum giving better reproducibility. A fuller explanation for the change from water

to acetone is given in another series of reports.[1] However, though the coating process was changed, the 10-micron powder was retained.

We were aware of the possibility that this particle size (10-microns) was not optimum. A typical comment on small spherical particles can be found in "Fundamentals of Ferromagnetism" here quoted:[2]

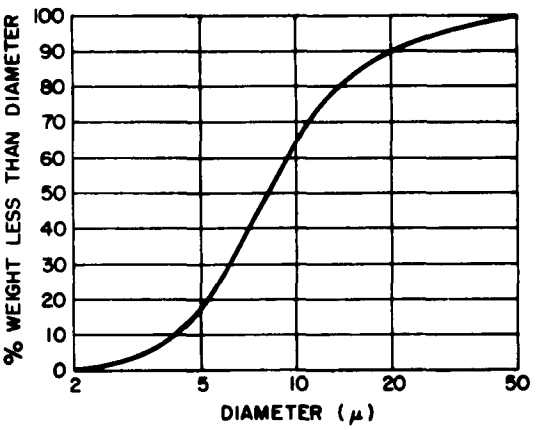

FIG.3-1 PARTICLE SIZE DISTRIBUTION ANALYSIS OF CARBONYL IRON, TYPE HP

> ... In order to decrease losses, it is common practice to use thin strips, thin sheets, or small particles insulated from one another.
>
> Spherical iron particles for high frequency work are obtained by chemical decomposition of iron carbonyl, and then "potted" in a low loss dielectric. These particles have the advantages of low loss because of small diameter and a large number of walls per unit distance.

After we had satisfied ourselves that we could constantly reproduce samples in small lots, we undertook the task of determining the effect of particle size on attenuation, resistance, and voltage breakdown.

---

[1] Mohrbach, P. F., Wood, Robert F., "RF Attenuating Material Studies (U)", The Franklin Institute Report P-A2301-19.

[2] Arrott, Anthony, Goldman, J. E. "Fundamentals of Ferromagnetism".

3.1.1 Comparison of Particles 5, 8, 10 and 20 Microns in Diameter

In addition to the standard 10-micron powder, carbonyl iron powders ranging in size from 5 to 20 microns were evaluated. The powders are all from the same manufacturer and were produced about the same time. All test specimens were made from 25 gram batches consisting of 99% carbonyl iron powder, 1% H_3PO_4, 10 cc of acetone, and then pressed at 85,000 psi. Our evaluation consisted of three samples from each of four batches of 5, 8, 10 and 20 micron powders. Results from the powders evaluated at 500 Mc are given in Table 3-1.

Table 3-1

EFFECT OF POWDER SIZE ON PARAMETERS

Diameter (Microns)	Density (gm/cm^3)	Attenuation at 500 Mc (db/cm)	Resistance (Megohms)	Breakdown* (Volts)
5	6.16	27	100	800
8	6.31	30	100	990
10	6.11	42	10	305
20	6.09	100	1	115

*In "standard" sample toroid configuration.

Data indicates that as particle size increases from 5 to 20 microns, the attenuation increases and the resistance decreases. Attenuation of the 5 micron powder is 27 db/cm; this increases with partical size to 100 db/cm at 20 microns (see Figure 3-2). The curve of density versus particle size rises to a peak at 8 microns and then falls off to 6.09 gm/cc at 20 microns (Figure 3-3). The voltage breakdown curve (Figure 3-4) has the same general shape as the density curve, both peaking at 8 microns.

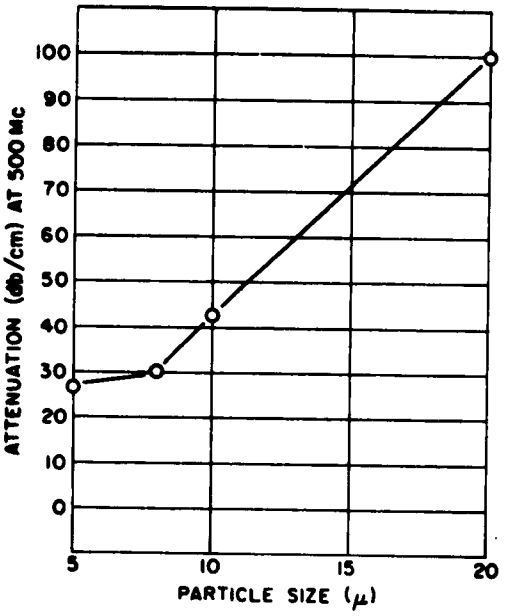

FIG. 3-2. PARTICLE SIZE VERSUS ATTENUATION

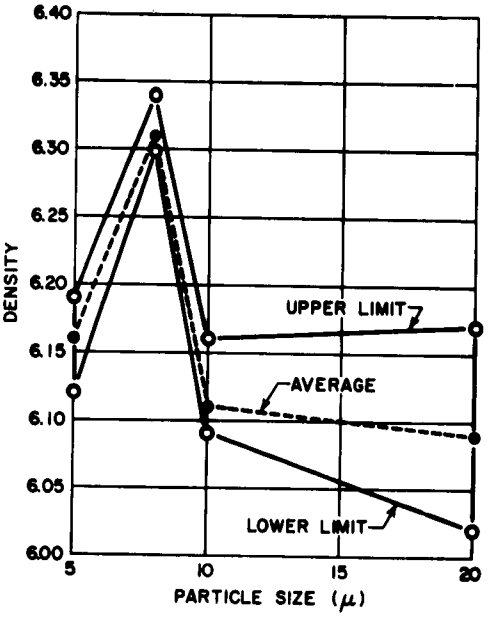

FIG. 3-3. PARTICLE SIZE VERSUS DENSITY

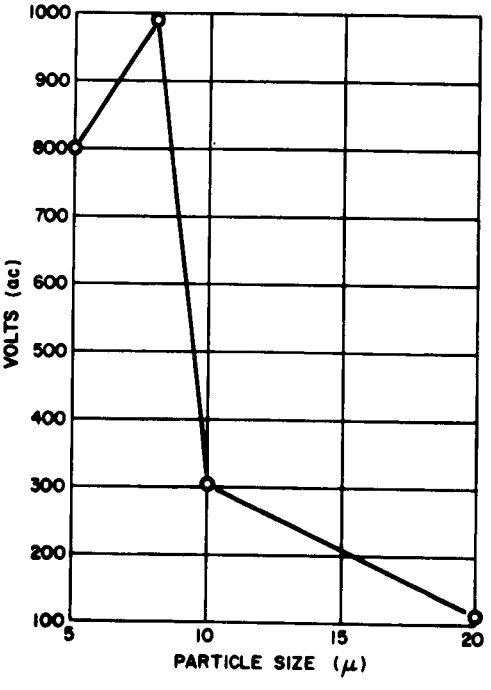

FIG. 3-4. PARTICLE SIZE VERSUS VOLTAGE BREAKDOWN

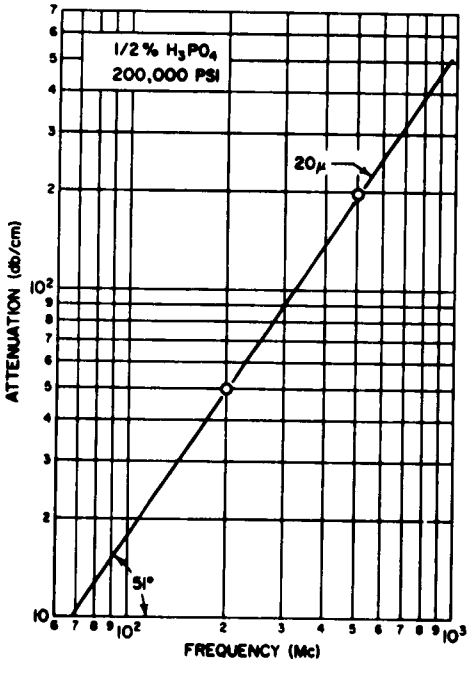

FIG. 3-5. ATTENUATION VERSUS FREQUENCY
(20 Micron Powder)

The data gathered from this experiment suggested that we might make a sample with very high attenuation by using the 20-micron powder and 1/2% insulation. We made several batches of 99.5% 20-micron iron powder and 1/2%, H_3PO_4. The attenuation at 200 Mc was 49 db/cm and at 500 Mc, 200 db/cm. These data are plotted in Figure 3-5.

3.1.2 Larger Particles of Carbonyl Iron

To continue our studies of particle size effects, we obtained a sample of unsized carbonyl iron powder and separated it ourselves, by means of the standard sieve series, into various particle sizes. Table 3-2 shows the percent by weight of a given particle size versus the particle diameter expressed in microns. Figure 3-6 illustrates the particle size distribution in graphical form.

Table 3-2

RAW CARBONYL IRON POWDER SIEVE SEPARATION

Mesh	Particle Size Microns*	Retained on Indicated Mesh	
		Wt. in Grams	%
20	>841	5.5	1.58
40	>360	49.0	14.04
60	>250	159.5	45.76
80	>177	48.0	13.76
100	>149	47.5	13.61
140	>110	18.5	5.30
200	>75	4.3	1.23
230	>68	6.0	1.72
325	>44	10.5	3.01
		348.8	100.00

*Particle size of fraction is greater than size listed, but less than next largest shown.

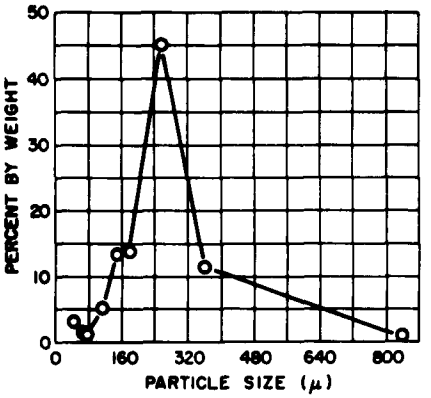

FIG. 3-6. PARTICLE SIZE DISTRIBUTION OF RAW CARBONYL IRON

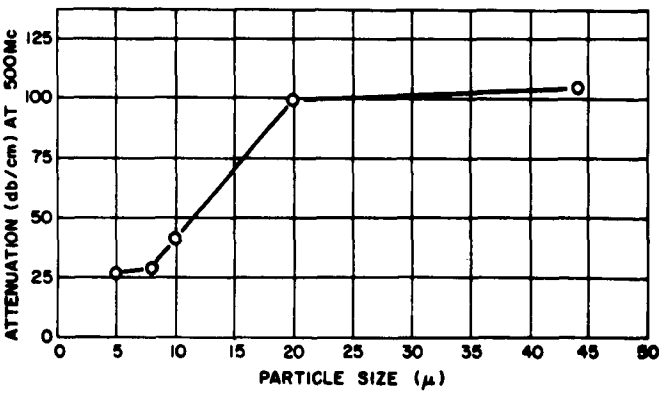

FIG. 3-7. PARTICLE SIZE vs. ATTENUATION

Results of attenuation measurements indicate that maximum attenuation for a sample composed of 99% carbonyl iron and 1% phosphoric acid and molded at 85,000 psi, occurs in specimens composed of 44 micron diameter powder.

Figure 3-7 shows that attenuation rises sharply as particle size increases from 5 to 44 microns. Above 44 microns, even 3% insulation did not produce the 500 ohm minimum dc resistance we require before measuring attenuation.

It will be noted from Figure 3-8 and the date in Table 3-3 that dc resistance drops as particle size increases. We feel that drop in resistance has little effect upon attenuation when the sample resistance is greater than 500 ohms. This may not be apparent from the present date, but on previous contracts we have made samples having various resistances and have observed that values above 500 ohms do not materially affect the measured attenuation if density is held constant. Below 500 ohms, the shunt resistance starts to influence the attenuation.

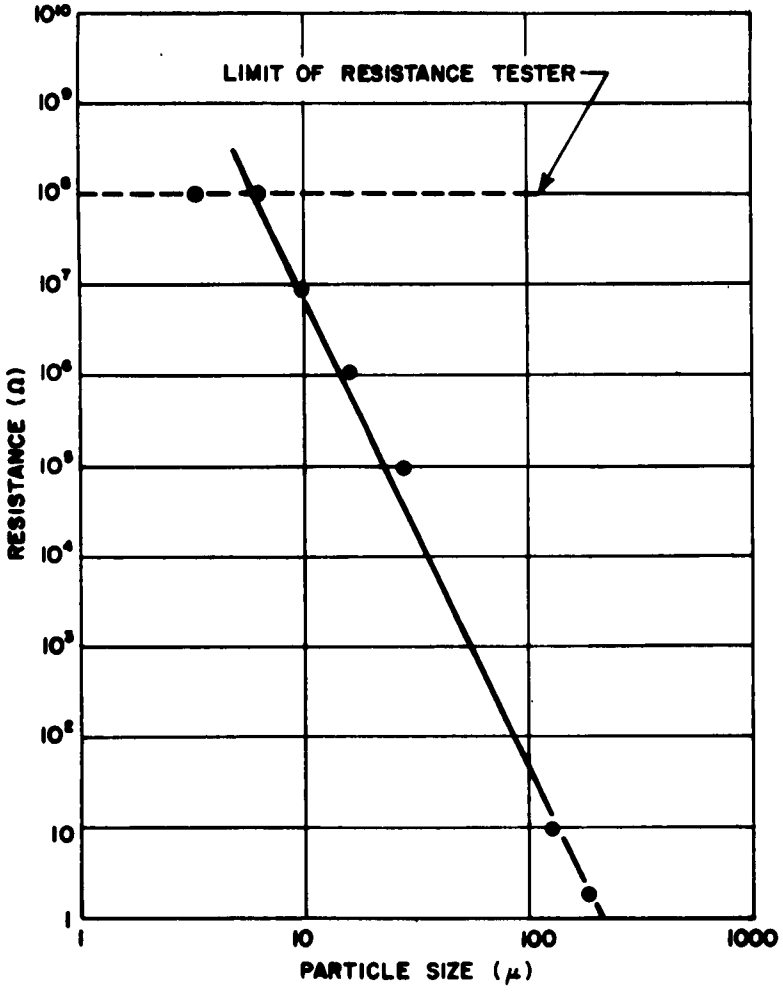

FIG. 3-8. RESISTANCE vs. PARTICLE SIZE

Table 3-3

SAMPLE CHARACTERISTICS

Particle Diameter Microns	Density gm/cm^3	dc Resistance Megohms	Breakdown Voltage	Attenuation (500 Mc) db/cm	Percent Insulation H_3PO_4
5	6.16	>100.0	800	27	1.0
8	6.31	>100.0	990	30	1.0
10	6.11	10.0	305	42	1.0
20	6.09	1.0	115	100	1.0
44	6.18	0.1	-	105	1.0
110	6.18	10Ω	-	-	1.0
177	5.70	1Ω	-	-	3.0
250	5.75	1Ω	-	-	3.0

3.2 Insulating of Carbonyl Iron

Our standard method of making attenuating material is to coat the iron particles using a phosphoric acid solutions. During the past year, we have tried several other methods of coating and have accumulated some interesting data.

3.2.1 Nitric Acid (HNO_3)

One of the most promising coating materials is nitric acid. Data taken at 500 Mc on samples coated with HNO_3 are shown in Table 3-4.

Table 3-4

MULTIPLE COATED SAMPLES

Coating Procedure	Attenuation 500 Mc db/cm	Voltage Breakdown	Resistance (megohms
1/2% + 1/4% HNO_3	96	116 volts	0.5
1/2% + 1/4% + 1/4% HNO_3	60	210 volts	1.0
1/2% + 1/2% + 1/2% HNO_3	40	300 volts	1.0

The technique of coating had to be modified when nitric acid was used; multiple coatings of low strengths were applied, rather than a single full-strength one.

From the data presented in Table 3-4, it would seem that this method of coating is comparable to our acetone-phosphate system. Unfortunately, this is not a fact. Samples made by this system are subject to oxidation, which we have been unable to prevent. This leads to a continual drop in attenuation over a period of time.

3.2.2 Hydrochloric Acid (HCl)

Samples made using HCl as the coating agent have been evaluated on a limited scale. Because HCl is highly corrosive to iron, it is difficult to form a coating. For samples that were successfully coated, only 4 db/cm of attenuation at 500 Mc could be realised.

3.2.3 Sulfuric Acid (H_2SO_4)

Sulfuric acid presents the same problem as hydrochloric; it is also highly corrosive to iron. A typical value for a sample made by this process follows:

Sample Number	Resistance	Attenuation (500 Mc)
4635	286 ohms	9.6 db/cm

3.2.4 Titanium Dioxide (TiO_2)

At this point, we deviated from acid-coating to coating with an insulating material having a high dielectric constant, hereafter called Hi-K material. A typical set of data obtained for samples coated with titanium dioxide (TiO_2) is shown in Table 3-5.

Table 3-5

TiO_2 COATED CARBONYL IRON SAMPLES

TiO_2 (1%)	Resistance (kilohms)	Density (gm/cm^3)	Attenuation at (500 Mc) (db/cm)	Breakdown (Volts)
2	0.05	6.32	*	*
3	3.1	6.15	64.9	100
4	300	6.03	40.4	140
5	500	6.00	38.8	155
6	650	5.86	29.4	235

*Not measured, resistance too low.

Results from this coating process compare favorably with our standard acetone-phosphate process in respect to attenuation. Resistance values in each lot (% of TiO_2) varied over a wide range. We do not plan to use this system in place of the acetone-phosphate system since it requires a much more elaborate and time-consuming process for producing the coating. This, taken with the difficulty of controlling the resistance from lot to lot, does not justify a shift in coating process.

3.2.5 Barium Titanate ($BaTiO_3$)

Data from the $BaTiO_3$ process follows closely that obtained with the TiO_2 system. Typical values obtained are those shown in Table 3-6.

Table 3-6

BARIUM TITANATE COATED SAMPLES

Sample Number	Resistance (ohms)	Density (gm/cm^3)	Attenuation at (500 Mc) (db/cm)	Breakdown Voltage
6404	105	6.45	-	-
6408	180 K	6.26	42.8	-
6427	62 M	6.27	56.8	155
6430	500 M	6.04	19.1	420

3.2.6 Other Coating Techniques

The coating processes that we have discussed in Section 3.2 are those that were carried out during this contract. In the course of work on other contracts, several other processes were investigated:

1. Water - phosphate
2. Silica
3. Silicone
4. Silicates (including glass)
5. Special coatings done at Picatinny Arsenal

None of these systems were equal to, or superior to our acetone-phosphate process.

3.3 Relationship of Density and Resistance to Attenuation

Evaluation of data dealing with the effects of particle size upon attenuation indicated that dc resistance and attenuation were in some way related. We noticed that resistance decreased while attenuation increased proportionately with increasing particle diameter. Additional experiments showed that the effects upon attenuation of particle diameter, density, and dc resistance are not readily separable.

To obtain a curve that would relate the three parameters (resistance, density, attenuation) we chose a formulation of 98.5% carbonyl iron powder and 1.5% H_3PO_4. To obtain a range of values for density, resistance, and attenuation, we varied the pressure which the samples were molded from 85,000 psi to 200,000 psi.

Figure 3-9 contains a graphical summary of the results. Attenuation, as illustrated by the curve, increases with decreasing resistance; but, density also increases as resistance decreases.

These data lead us to believe that both decreased resistance and increased density are operating conjointly and indistinguishably to

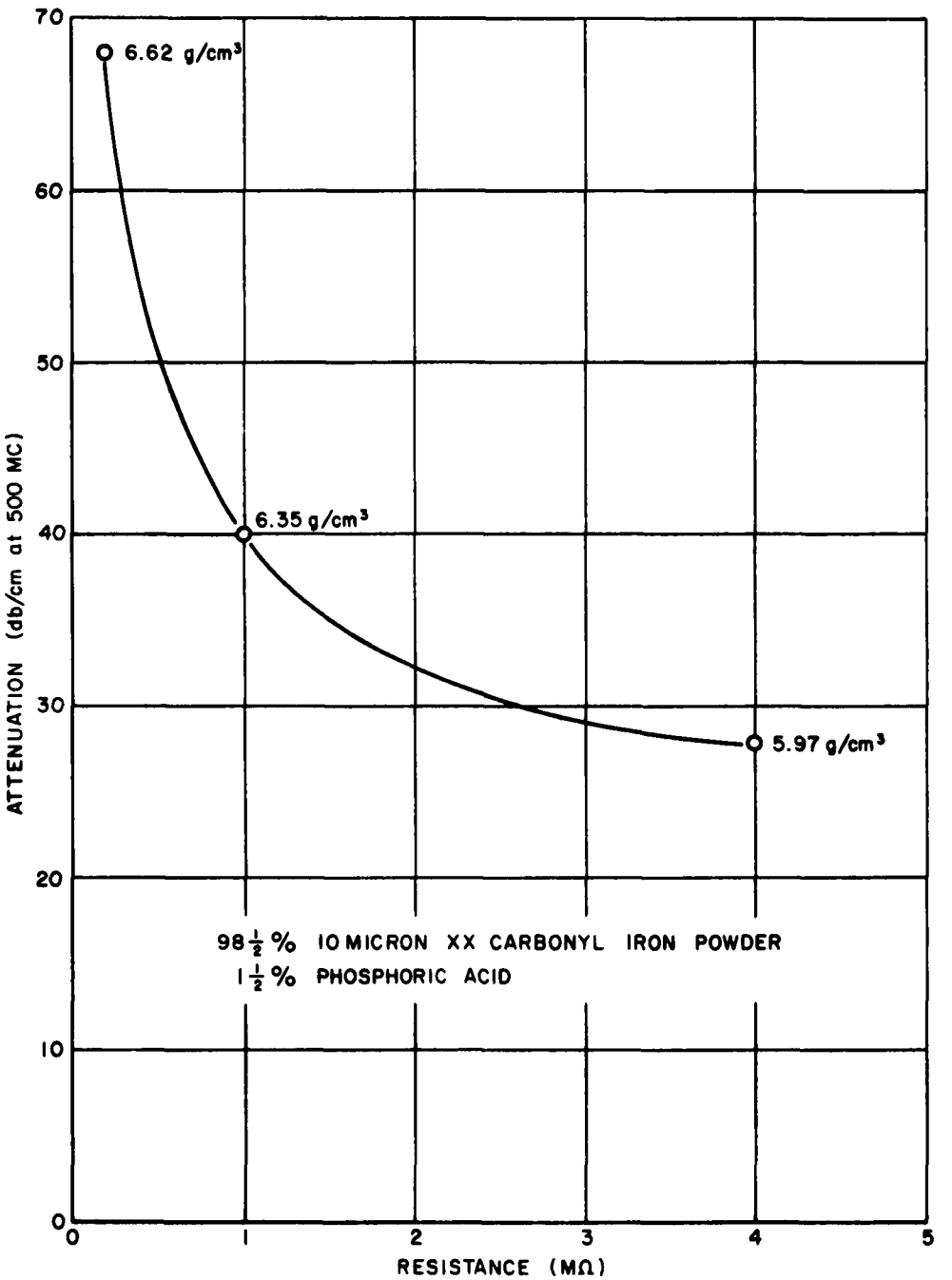

FIG. 3-9. RESISTANCE VERSUS ATTENUATION

increase the attenuation of our samples. The effects of density and resistance are interdependent. When the pressure at which a sample is being fabricated is increased, the density is increased and a corresponding decrease in resistance is observed. This is because the insulated iron particles are more closely packed (possibly deformed) or because the insulation fails mechanically under the increasing pressure, or both. In either case, the density and hence the attenuation, increase as resistance decreases.

3.4 Summary of Chemical Studies of Carbonyl Iron

Using our present acetone-phosphate technique, carbonyl iron powder cannot be insulated with less than 0.5% H_3PO_4, this limit being marked by a large drop in dc resistance. Increasing the percentage of insulation to 1.5% causes a proportional increase in dc resistance. Beyond this point, dc resistance will not increase and may actually drop off. The voltage breakdown of a sample will also increase with increasing insulation until the 3.0% mark is reached. We have not investigated phosphate insulation beyond the 3% mark because the attenuation at 500 Mc drops off rather rapidly from 40 db/cm at 0.5% insulation to 10 db/cm at 3% insulation.

An insulation coating of 1% H_3PO_4 results in a dc resistance of 500 megohms for 5 micron powders and 1.5 megohms for 20 micron powders. This, we believe, is due to the large surface area (for a given weight) of the smaller particles and the rate of chemical reaction. The acid is assumed to be more evenly distributed over the large surface area and, hence, we have many uniformly insulated spheres. When we go to the larger particles, we have fewer particles (for a given weight) and considerably less surface area. Therefore, the acid is not being used as efficiently as with the smaller particles and consequently we get a lower resistance.

Physical properties of the raw powder have a great deal to do with the insulation characteristics of the coated powder. As an example, if the powder particles are non-spherical in shape, we have difficulty in coating them. When these powders are pressed, their irregularities tend to puncture the insulation and thus give an extremely low resistance. Similarly, large spherical particles are more easily deformed by pressure than are small ones. When these particles are deformed, the insulation cracks and the resistance drops into the low megohm range.

3.5 Other Powders

Iron powder made by the carbonyl process has been the basic ingredient used during our development of an RF attenuating material. Since iron is ferromagnetic, we decided to try other ferromagnetic powders to see if a more lossy attenuator could be made. Toward this end, we have conducted experiments utilizing nickel, alnico mixture, sponge iron and one paramagnetic material - zinc.

3.5.1 Nickel Powders

Five samples of nickel powder were obtained. They are all 177 microns or less in diameter and were produced by different processes (electrolytically annealed, chemically precipitated, and reduced oxides). We were not able to insulate the nickel powders by materials already in use, such as H_3PO_4, HNO_3, SiO_2. An attempt was made to insulate the particles by oxidizing the surface, by heating in the presence of oxygen. Results were poor, as we were unable to obtain sufficient resistance to enable us to measure the attenuation of the samples. We believe that our inability to form an insulating coat is due to the irregular shape of the particles.

A second method consisted of trying to coat the nickel particles with nickel nitrate. Nickel nitrate was made by heating nickel and an excess of nitric acid in isopropyl alcohol. We had no success in producing samples with more than a few ohms resistance.

3.5.2 Alnico Powder

We were very desirous of evaluating alnico as a source of attenuating material because it is more ferromagnetic than iron. However, we could not find a source of the powder. An effort is being made by various manufacturers to make alnico in powder form and it may be available in the future.

We mixed the required elements in an attempt to form alnico powder. Samples made from these mixtures had a resistance of about 5 ohms. Furthermore, they grow with time, and therefore, do not fit into our attenuation measuring system.

3.5.3 Sponge Iron Powders

Investigation of sponge iron powder as a substitute for carbonyl iron was aimed not so much at increasing attenuation as at finding another source of iron powder. We evaluated three types of sponge iron that were insulated by our acetone-phosphate process.

Data obtained are tabulated in Table 3-7.

Table 3-7

COMPARISON OF SPONGE IRON POWDERS

Type	Density (gm/cm^3)	Attenuation at (500 Mc) (db/cm)	Resistance (kilohms)	Breakdown (Volts, RMS)
EP 1024	-	-	0.03	-
MH 300	6.35	40	25.	30
A-EP1024	6.37	38	1000.	30

From the standpoint of attenuation and resistance, type A-EP1024 appears to be a satisfactory substitution for carbonyl iron. However, the voltage breakdown is very low, only 30 volts.

3.5.4 Zinc Powder

A small effort during this past year was directed toward the investigation of zinc and its oxide. We did this to observe the behavior of a paramagnetic metal. Again, we were not able to insulate the powder.

4. APPLIED STUDIES

4.1 Dielectric Cap Studies

Contributor: James D. Dunfee

RF attenuating materials used to envelope initiator conductors frequently have low resistance and low voltage breakdown. Use of a Formvar insulating film (0.0003 to 0.0005 inches in thickness) baked on the conductors can be used to increase both of these properties; however, this reduces the RF attenuation of the insulated assembly by 60 percent.

Theoretical analysis predicts that an insulating layer can be interposed between the conductors and the attenuating material without an appreciable loss in attenuation provided the dielectric constant and insulation thickness are properly specified. The range of permittivity values required for successful application of such a film appears to be available in barium and other titanate ceramics. We obtained from a commercial manufacturer a large number of tubular capacitor bodies in a wide range of permittivities. A testing program during the past year was directed toward establishing the values of dielectric constant and thickness of insulation which do not seriously reduce the attenuation of the insulated assembly. Most of the insulated assemblies were made with the tubular ceramic bodies previously mentioned.

The general testing procedure consists of first measuring the RF attenuation of a carbonyl iron attenuating sample in a coaxial line as shown in Figure 4-1. Next, a ceramic tubular capacitor body with a specified permittivity is cemented on a brass center conductor using a silver-filled conductive epoxy cement. After curing the cement, the ceramic tube is cylindrically ground to a specified thickness. Another carbonyl iron sample with density, thickness, and other characteristics similar to the first sample is then bored to precise dimensions, fitted, and cemented over the ceramic insulating tube. The completed assembly is shown in Figure 4-2. Besides fixing the relative position of the component parts of the assembly, the silver epoxy cement is used to prevent the RF from passing through the air spaces between the fitted parts. The final step in the test procedure is the measurement of the RF attenuation of the insulated assembly; the result is compared with that obtained with the uninsulated assembly, and the percentage change calculated.

A series of tests were conducted with various thicknesses of ceramic tubing and a wide range of values of the dielectric constant. Results of these tests are shown in Figure 4-3. It can be seen that decreasing the material thickness and increasing the dielectric constant of the insulator reduces the adverse effect upon attenuation using uninsulated models as standards of comparison. A ceramic with a dielectric constant greater than 115 and a thickness of 0.017 inch can be inserted between the carbonyl iron attenuator and the center conductor without impairing the attenuation. At the other extreme, the curve for glass bonded mica with a dielectric constant of 7 shows 2 75% drop in attenuation with a thickness of 0.010 inch.

Some irregularities in the data for attenuation loss using ceramics with a dielectric constant of 82, indicated that physical properties other than the ceramic permittivity and thickness should also be measured. Measurements of the capacity and dissipation factors

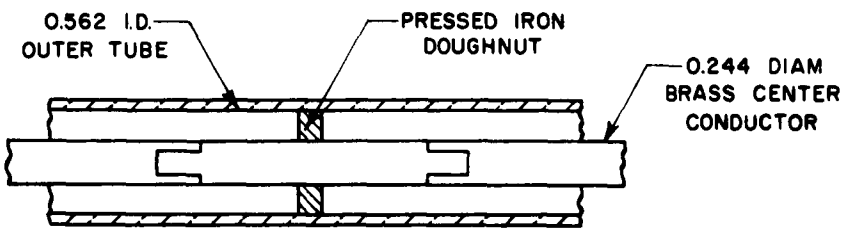

FIG. 4-1. ATTENUATING SAMPLE MOUNTED IN COAXIAL AIR LINE

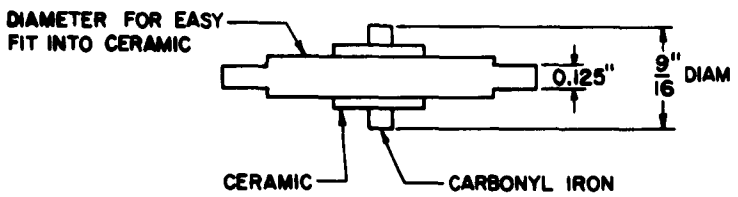

FIG. 4-2. CERAMIC INSULATOR ASSEMBLY

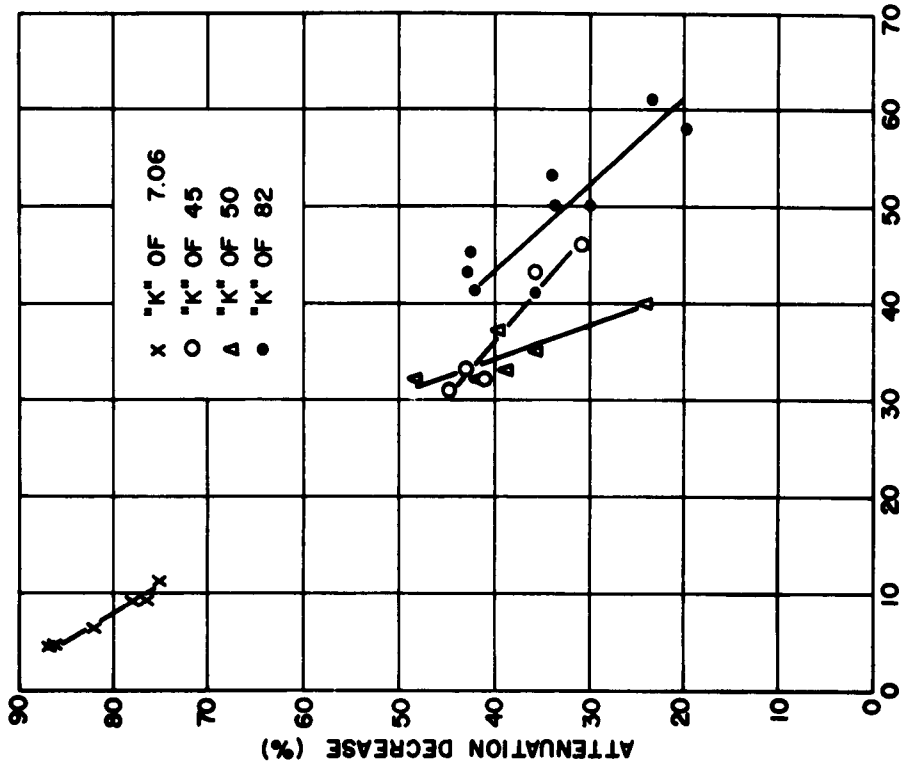

FIG. 4-4. CAPACITY – ATTENUATION CHANGE

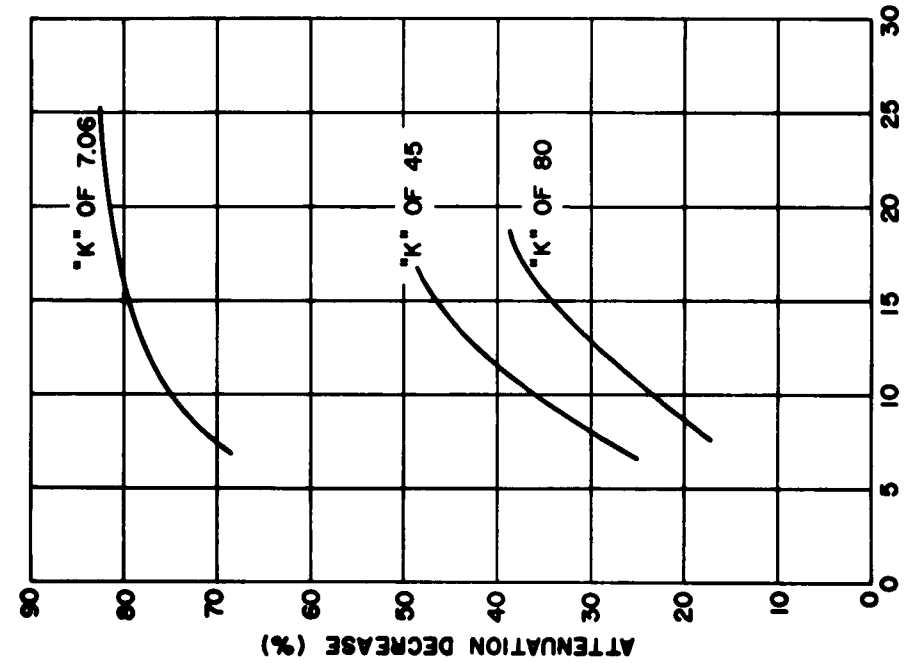

FIG. 4-3. ATTENUATION DECREASE vs. INSULATION THICKNESS

of the ceramics, attenuating materials, and assemblies were made. The assembly capacity is plotted versus attenuation drop in Figure 4-4. Increased capacity of the assembly reduces loss in attenuation. Capacity is, of course, a function of material thickness, dielectric constant, and effective area of the capacitor. Having investigated the first two variables, we varied the third, the area of the dielectric insulator. An area increase was accomplished by extending the silver coating past the edge of the iron sample as shown in Figure 4-5. By silvering the extending ceramic, we were able to increase capacity and attenuation up to the point where it was at the same level as the uninsulated assembly used for comparison purposes. The only explanation that we have at this time is that the added attenuation is supplied by the losses in the dielectric material.

To extend the data into the realm of practical wire size, a special sample group was fabricated using a very small lead zirconate ceramic tube (1/16 inch outside diameter x 1/32 inch inside diameter x 1/10 inch long) as an insulator, as shown in Figure 4-6. The carbonyl iron compact was molded in position on the ceramic tube, with the wire in place. Additional samples with a 1/16-inch diameter brass rod as a center conductor, having no insulation, were molded and used for comparison. No significant difference in attenuation was found between the two types of assemblies.

During the year, most of the data was obtained at a test frequency of 500 megacycles. Evaluation at frequencies down to 200 megacycles, with a variety of attenuating materials, gave similar results (See Figure 4-7 and Table 4-1). As can be seen in Figure 4-8, those were some unexpected changes in attenuation that could not be accounted for.

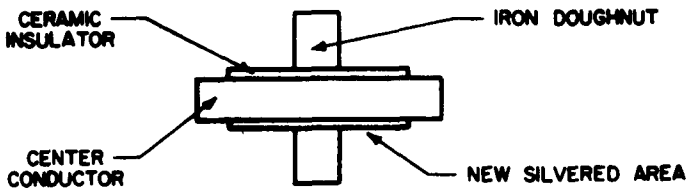

FIG. 4-5. INCREASING SAMPLE CAPACITY BY SILVERING

While irregularities were noted, it appears that insertion of a high permittivity dielectric between the initiator conductors and the attenuating material can be accomplished by the use of ceramic preforms, with little or no attenuation loss. Ceramic preforms do not, however, lend themselves to most initiator designs; therefore, we felt that a method of applying a film of ceramic material to the conducting wires

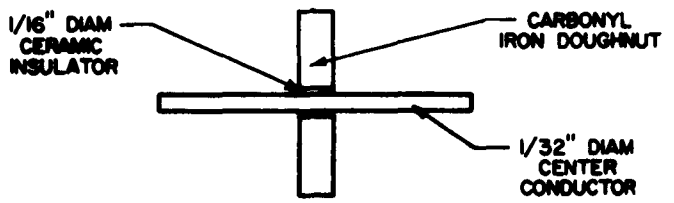

FIG. 4-6. SAMPLE DESIGN USING SMALL CERAMIC INSULATER

and to the inner portion of the initiator case itself should be developed. Further work at a wide range of frequencies, especially down to 1 Mc, should be performed to make certain that attenuation holds over the working range of frequencies, without gaps, thus decreasing the effectiveness of the attenuator. If the answers to these questions can be found, the resistances and voltage breakdown characteristics of the initiator assemblies at the attenuator plug cross-section can be specified independently of the attenuator material.

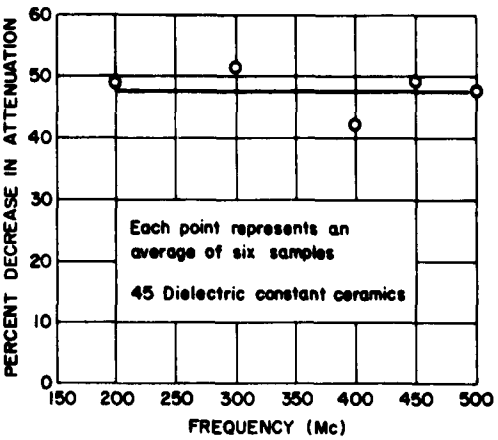

FIG. 4-7 ATTENUATION - FREQUENCY CURVE
(Percent decrease)

Paul F. Mohrbach
Project Leader

Robert F. Wood
Project Engineer

Approved by

E. E. Hannum
Applied Physics Laboratory

Francis L. Jackson
Director of Laboratories

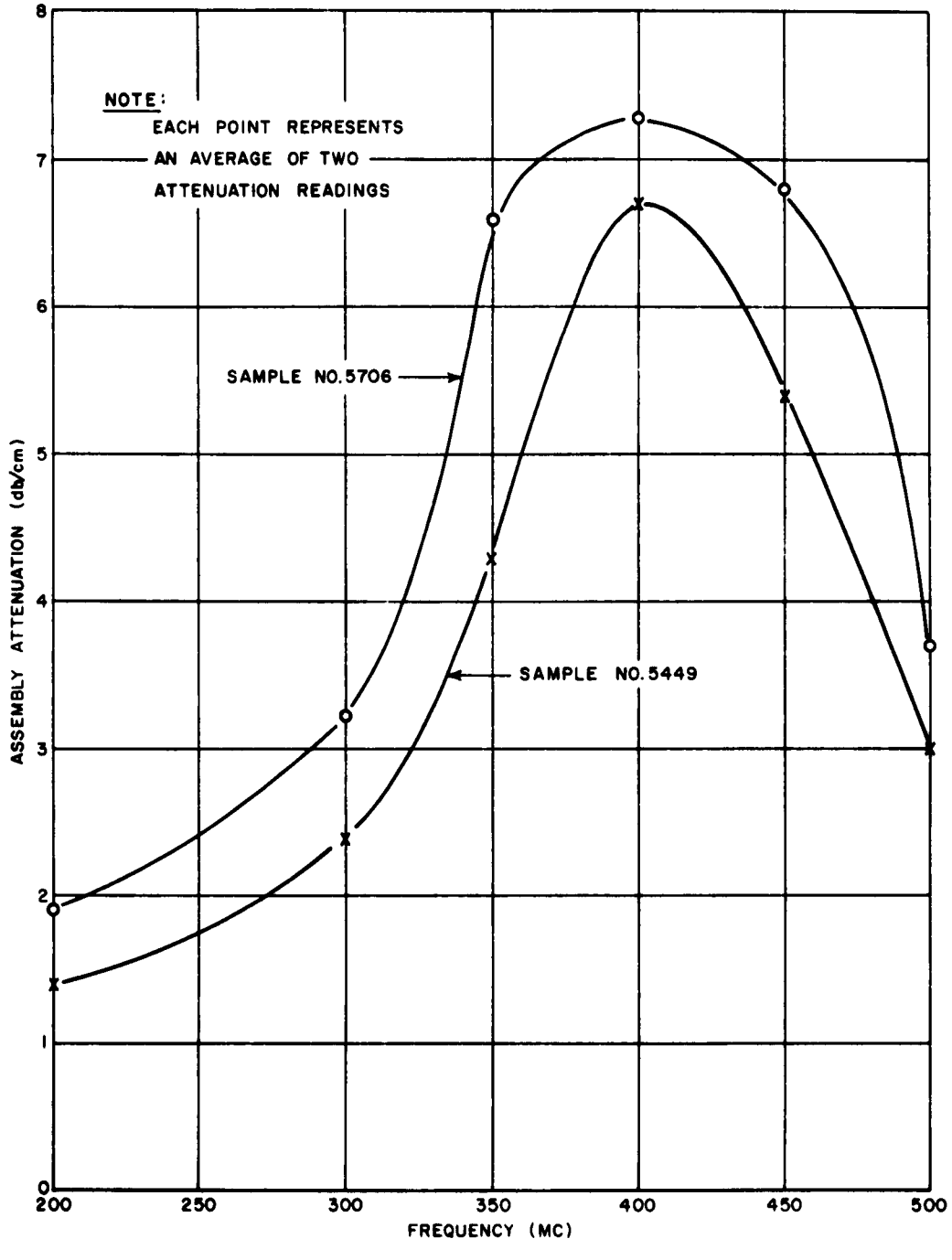

FIG. 4-8. ASSEMBLY ATTENUATION VERSUS FREQUENCY FOR GLASS BONDED MICA (K = 7) SAMPLES

APPENDIX A

RELATION OF μ^* PARAMETERS TO PARAMETERS HAVING A REAL μ

In the following equations, subscripts one (1) refer to the complex μ parameters and subscripts two (2) refer to the non complex μ parameters. The relationships were derived by equating the squares of the propagation constant and the characteristic impedance in the two systems.

$$\gamma_1^2 = -\omega^2 \mu_1^* \epsilon_1^* = \gamma_2^2 = -\omega^2 \mu_2 \epsilon_2^* \tag{1}$$

$$Zo_1^2 = \frac{\mu_1^*}{\epsilon_1^*} = Zo_2^2 = \frac{\mu_2}{\epsilon_2^*} \tag{2}$$

These equations yield four equations in three unknowns; the solutions give

$$\epsilon_2' = \sqrt{\frac{\left(\mu_1'\epsilon_1' - \mu_1''\epsilon_1''\right)^2 \left(\mu_1'\epsilon_1'' - \mu_1''\epsilon_1'\right)}{\left(\left(\mu_1'\right)^2 + \left(\mu_1''\right)^2\right)\left(\mu_1'\epsilon_1'' + \mu'' \epsilon_1'\right)}} \tag{3}$$

$$\epsilon_2'' = \sqrt{\frac{\left(\mu_1'\epsilon_1''\right)^2 - \left(\mu_1''\epsilon_1'\right)^2}{\mu_1'^2 + \mu_1''^2}} \tag{4}$$

$$\mu_2' = \sqrt{\frac{\left[\left(\mu_1'\right)^2 + \left(\mu_1''\right)^2\right]\left(\mu_1''\epsilon_1' + \mu_1'\epsilon_1''\right)}{\mu_1' \epsilon_1'' - \mu_1'' \epsilon_1'}} \tag{5}$$

where

$$\mu_1^* = \mu_1' - j\mu_1''$$
$$\epsilon_1^* = \epsilon_1' - j\epsilon_1'' \qquad (6)$$
$$\epsilon_2^* = \epsilon_2' - j\epsilon_2''$$
$$\mu_2 = \mu_2$$

Conductivity is expressed by the relationship

$$\sigma_2 = \epsilon_2'' \omega \qquad (7)$$

and is therefore equal to eq. 4 multiplied by ω.

DISTRIBUTION LIST

Commander
U.S. Naval Weapons Laboratory
Dahlgren, Virginia
Attn: Code WHR, Lyde Pruett (5)

Contracting Officer
U.S. Naval Weapons Laboratory
Dahlgren, Virginia
Attn: Code SSCP

Office of Naval Research
University of Pennsylvania
Rm. 213, Hare Building
Philadelphia 4, Penna.
Attn: Mr. R. L. Keane

Chief, Naval Operations (OP-411H)
Department of the Navy
Washington 25, D.C.

Chief, Bureau of Naval Weapons
Department of the Navy
Washington 25, D.C.
Attn: Code C-132
Attn: Code RAAV-3421
Attn: Code RM-15
Attn: Code RMMO-224
Attn: Code RMMO-235
Attn: Code RMMO-32
Attn: Code RMMO-33
Attn: Code RMMO-4
Attn: Code RMMO-43
Attn: Code RMMO-44
Attn: Code RMMP-343
Attn: Code RREN-312
Attn: Code DIS-313 (4)

Chief, Bureau of Medicine and Surgery
Department of the Navy
Washington 25, D.C.
Attn: Code 74

Chief, Bureau of Yards and Docks (Code D-200)
Department of the Navy
Washington 25, D.C.

Commander
U.S. Naval Ordnance Laboratory
White Oak, Maryland
Attn: Code ED
Attn: Code NO
Attn: Code LV
Attn: Code Technical Library

Commander
U.S. Naval Ordnance Laboratory
Corona, California
Attn: Code 561
Attn: Code 552

Commander
U.S. Naval Ordnance Test Station
China Lake, California
Attn: Code 556
Attn: Code 4572

Commanding Officer
U.S. Naval Air Development Center
Johnsville, Pennsylvania
Attn: Code EL-94

Commanding Officer
U.S. Naval Underwater Ordnance Station
Newport, Rhode Island

Director
U.S. Naval Research Laboratory
Washington 25, D.C.
Attn: Code 5439
Attn: Code 5410 (2)

Commanding Officer
U.S. Naval Nuclear Ordnance
Evaluation Unit
Kirtland Air Force Base
Albuquerque, New Mex
Attn: Code 40

Commandant of the Marine Corps
Washington 25, D.C.
Attn: Code A04C

DISTRIBUTION LIST (Cont.)

Commander
Pacific Missile Range
P.O. Box 8
Point Mugu, California
Attn: Code 3260

Commanding Officer and Director
U.S. Navy Electronics Laboratory
San Diego 52, California
Attn: Code Library

Commanding Officer
U.S. Naval Ordnance Plant
Macon, Georgia
Attn: Code PD 270

Commander Naval Air Force
U.S. Atlantic Fleet CNAL 724B
U.S. Naval Air Station
Norfolk 11, Virginia

Commander Service Force
U.S. Atlantic Fleet
Building 142, Naval Base
Norfolk 11, Virginia

Commander Training Command
U.S. Pacific Fleet
c/o U.S. Fleet Anti-Submarine
Warfare School
San Diego 47, California

Commanding General
Headquarters, Fleet Marine Force,
Pacific
c/o Fleet Post Office
San Francisco, California
Attn: Force Communications
Electronic Officer

Commander in Chief
U.S. Pacific Fleet
c/o Fleet Post Office
San Francisco, California
Attn: Code 4

Commander Seventh Fleet
c/o Fleet Post Office
San Francisco, California

Commander
New York Naval Shipyard
Weapons Division,
Naval Base
Brooklyn 1, New York
Attn: Code 290
Attn: Code 912B

Commander
Philadelphia Naval Shipyard
Naval Base
Philadelphia 12, Penna.
Attn: Code 273

Commander
Pearl Harbor Naval Shipyard
Navy No. 128, Fleet Post Office
San Francisco, California
Attn: Code 280

Commander
Portsmouth Naval Shipyard
Portsmouth, New Hampshire

Department of the Army
Office Chief of Ordnance
Washington 25, D.C.
Attn: Code ORDGU-SA
Attn: Code ORDTN
Attn: Code ORDTB (Research &
Special Projects)

Office Chief Signal Officer
Research and Development Division
Washington 25, D.C.
Attn: Code SIGRD-8

Commanding Officer
Diamond Ordnance Fuze Laboratories
Washington 25, D.C.
Attn: Mr. T. B. Godfrey

DISTRIBUTION LIST (Cont.)

U.S. Army Nuclear Weapon
Coordination Group
Fort Belvoir, Virginia

Director
U.S. Army Engineer Research
and Development Labs.
Fort Belvoir, Virginia
Attn: Chief, Basic Res. Group

Commanding Officer
Picatinny Arsenal
Dover, New Jersey
Attn: Artillery Ammunition &
Rocket Development
Laboratory -
Mr. S. M. Adelman

Commanding Officer
U.S. Army Environmental Health
Laboratory
Building 1235
Army Chemical Center, Maryland

Commanding General
Headquarters 2DRAADCOM
Oklahoma City, AFS
Oklahoma City, Oklahoma

Commanding Officer
U.S. Army Signal Research &
Development Laboratory
Fort Monmouth, New Jersey
Attn: SIGEM/EL-GF

Commander
U.S. Army Rocket and Guided
Missile Agency
Redstone Arsenal, Alabama
Attn: ORDXR-R (Plans)

Commanding Officer
Office of Ordnance Res., U.S. Army
Box CM, Duke Station
Durham, North Carolina
Attn: Internal Research Division

Commanding General
White Sands Missile Range
New Mexico
Attn: Code ORDBS-G3

Commanding Officer
White Sands Missile Range,
New Mexico
U.S.A. SMSA
Attn: Code SIGWS-AJ (4)

Commanding General
U.S. Army Electronic Proving Ground
Ft. Huachuca, Arizona
Attn: Technical Library

Director of Office of Special
Weapons Development
U.S. Continental Army Command
Fort Bliss, Texas
Attn: Capt. Chester I. Peterson
T S Control Officer

Headquarters
Air Research & Development Command
Andrews Air Force Base
Washington 25, D.C.
Attn: Code RDMMS-3

Commander
Air Force Missile Test Center
Patrick Air Force Base, Florida
Attn: Code MTRCF

Headquarters Ogden Air Material Area
Hill Air Force Base
Ogden, Utah
Attn: Code OOYSS

Commander, Charleston Naval Shipyard
U.S. Naval Base
Charleston, South Carolina

Griffiss Air Force Base
RADC New York
Attn: RCLS/Philip L. Sandler

DISTRIBUTION LIST (Cont.)

Commander
Air Force Special Weapons Center
Kirtland Air Force Base
Albuquerque, New Mexico
Attn: Code SWVSA

Commanding General
Air Fleet Marine Force, Pacific
MCAS, El Toro
Santa Ana, California

Commander
Headquarters Ground Electronics
Engineering Installation Agency
Griffiss Air Force Base
Rome, New York
Attn: Code ROZMWT

Armed Services Explosives Safety
Board
Department of Defense
Room 2075, Bldg. T-7, Gravelly Point
Washington 25, D.C.

Headquarters
Armed Services Technical Information
Agency
Arlington Hall Station
Arlington 12, Virginia
Attn: TIPCR (10)

Commander
Field Command
Defense Atomic Support Agency
Albuquerque, New Mexico
Attn: Code FCDR3

Defense Research Staff
Brittish Embassy
3100 Massachusetts Ave., N.W.
Washington 8, D.C.
Attn: Mr. G. R. Nice
VIA: Chief, Bureau of Naval Weapons
Department of the Navy
Washington 25, D.C.
Attn: Code DSC-3

Naval Member
Canadian Joint Staff
2450 Massachusetts Ave., N.W.
Washington 8, D.C.
Attn: Staff Officer (Weapons)
VIA: Chief, Bureau of Naval Weapons
Department of the Navy
Washington 25, D.C.
Attn: Code DSC-3

Aerojet-General Corporation
P.O. Box 1947
Sacramento, California
Attn: R. W. Froelich, Dept. 6620,
POLARIS Program

American Machine and Foundry Co. -
Alexandria Div.
1025 North Royal Street
Alexandria, Virginia
Attn: Dr. L. F. Dytrt

Atlas Powder Company
Reynolds Ordnance Section
P.O. Box 271
Tamaqua, Pennsylvania
Attn: Mr. R. McGirr

The Bendix Corporation
Scintilla Division
Sidney, N.Y.
Attn: R. M. Purdy

Bermite Powder Company
22116 West Soledad Canyon Road
Saugus, California
Attn: Mr. L. LoFiego

Bethlehem Steel Company, CTD
97 E. Howard Street
Quincy, Massachusetts
Attn: Mr. W. C. Reid

DISTRIBUTION LIST (Cont.)

Chance Vaught Corporation
P.O. Box 5907
Dallas 22, Texas
Attn: R. D. Henry

The Franklin Institute
20th Street and Benjamin
Franklin Parkway
Philadelphia 3, Penna.
Attn: Mr. E. E. Hannum, Head
Applied Physics Lab.

Grumman Aircraft Engineering Corp.
Weapons Systems Department
Bethpage, Long Island, New York
Attn: Mr. E. J. Bonah

Jansky and Bailey, Inc.
1339 Wisconsin Avenue, N.W.
Washington, D.C.
Attn: MR. F. T. Mitchell, Jr.

Librascope Division
General Precision, Inc.
670 Arques Avenue
Sunnyvale, California
Attn: Mr. R. Carroll Maninger

Lockheed Aircraft Corporation
P.O. Box 504
Sunnyvale, California
Attn: Missile Systems Division,
Dept. 62-20
Mr. I. B. Gluckman
Attn: Missiles and Space Division,
Dept. 81-62
Mr. E. W. Tice
Attn: Missiles and Space Division,
Dept. 81-71
Mr. R. A. Fuhrman

McCormick Selph Associates
Hollister, California
Attn: Technical Librarian

Midwest Research Institute
425 Volker Boulevard
Kansas City, Missouri
Attn: Security Officer
Mr. C. M. Fisher

RCA Service Company
Systems Engineering Facility
Government Service Department
838 N. Henry Street
Alexandria, Virginia

Sandia Corporation (Div. 1262)
Albuquerque, New Mexico
VIA: FCDASA

University of Denver
Denver Research Institute
Denver 10, Colorado
Attn: Mr. R. B. Feagin

U.S. Flare Division Atlantic Res.
Corporation
19701 W. Goodvale Road
Saugus, California
Attn: Mr. N. C. Eckert, Head,
R&D Group

Aerojet-General Corporation
P.O. Box 296
Azusa, California
Attn: M. Z. Grenier, Librarian

Welex Electronics Corporation
Solar Building, Suite 201
16th and K Streets, N.W.
Washington 5, D.C.

North American Aviation, Inc.
Communications Services
4300 East 5th Ave.
Colorado 16, Ohio

DISTRIBUTION LIST (Cont.)

Commander
U.S. Army Ordnance
Frankford Arsenal
Philadelphia 37, Penna.

U.S. Atomic Energy Commission
Division of Military Application
Washington 25, D.C.

U.S. Naval Explosive
Ordnance Disposal Facility
U.S. Naval Propellant Plant
Indian Head, Maryland

The Martin Company
P.O. Box 5837
Orlando, Florida
Attn: Engineering Library

Commanding Officer
Picatinny Arsenal
Dover, New Jersey
Attn: SMUPA-VP3,
Plastics Technical
Evaluation Center,
A. M. Anzalone (2)